NUREG/CR-0721

LMFBR FUEL ANALYSIS
TASK A: OXIDE FUEL DYNAMICS

Final Report
October 1977 - September 1978

V. K. Dhir W. E. Kastenberg
M. Frank T. E. McKone

University of California, Los Angeles

Prepared for
U. S. Nuclear Regulatory Commission

Available from
National Technical Information Service
Springfield, Virginia 22161
Price: Printed Copy $6.00 ; Microfiche $3.00

The price of this document for requesters outside of the North American Continent can be obtained from the National Technical Information Service.

NUREG/CR-0721

LMFBR FUEL ANALYSIS
TASK A: OXIDE FUEL DYNAMICS

Final Report
October 1977 - September 1978

V. K. Dhir W. E. Kastenberg
M. Frank T. E. McKone

University of California, Los Angeles
Department of Chemical, Nuclear and Thermal Engineering
Los Angeles, CA 90024

Manuscript Completed: March 1979
Date Published: March 1979

Prepared for
Division of Project Management
Office of Nuclear Reactor Regulation
U. S. Nuclear Regulatory Commission
Washington, D.C. 20555
Under Contract No. NRC 03-77-001

PREFACE

The report presented here represents a summary of work accomplished as part of the Technical Assistance Program, U.S. Nuclear Regulatory Commission, Division of Project Management. In particular, this final report for the period October 1, 1977 - September 30, 1977, (TASK A: Oxide Fuel Dynamics) is concerned with generic questions relating to the behavior of oxide fuel in LMFBR's during postulated unprotected overpower transients. In addition, a small section is devoted to some safety questions related to alternative fuels.

The help of Drs. J. F. Meyer and T. Speis of the Nuclear Regulatory Commission staff is greatly acknowledged. Several of our graduate students (V. Badham, F. Rahnema, B. Hauss and I. Shokar) were very helpful in conducting literature searches and in computer programming. The models and computer code used in the evaluation of internal fuel pin motion were developed under the support of the Electric Power Research Institute as part of the Ph.D. dissertation of M. Frank. The models and computer code used in the analysis of fuel plugging and freezing were developed under the support of the Division of Reactor Safety Research as part of the Ph.D. dissertation of K. Wong.

The report presented here is the sixth in a series of final reports as follows:

1. "Transient Analysis of LMFBR Oxide Fuel Elements During Accidents," R. C. Erdmann, UCLA-ENG-7362, August 1973.
2. "Transient Analysis of LMFBR Oxide Fuel Elements During Accidents," W. E. Kastenberg, UCLA-ENG-7468, August 1974.
3. "Preliminary Analysis of the Transient Overpower Accident for CRBRP," W. E. Kastenberg and M. Frank, UCLA-ENG-7557, July 1975.

4. "LMFBR Fuel Analysis, Task A: Oxide Fuel Dynamics," Final Report for the Period July 1, 1975 - September 30, 1976, NUREG-0146, January 1977.

5. "LMFBR Fuel Analysis, Task A: Oxide Fuel Dynamics," Final Report for the Period October 1, 1976 - September 30, 1977, NUREG/CR-0011.

Abstract

In this report, three aspects of LMFBR safety are discussed. The first concerns the potential reactivity effects of whole core fuel motion prior to pin failure in low ramp rate transient overpower accidents. The second concerns the effects of flow blockages following pin failure on the coolability of a core following an unprotected overpower transient. The third aspect concerns the safety related implications of using Thorium based fuels in LMFBR's.

Prefailure fuel motion was found to have a larger reactivity effect at high burnups because of the larger central cavity, and as plutonium builds up in the outer regions the radial power peaks toward the outer core region.

Following a transient overpower accident, severely restricted flow conditions in the coolant channel may lead to bulk boiling of sodium in the channels below the blockage on the order of one second. As a result of bulk boiling of sodium beneath the blockage, coolability of the porous blockage may be severely limited. Melting times between 1 and 10 minutes are possible, depending upon the location of the blockage.

A major problem in determining the safety implications of using thorium based fuels is the lack of data. In particular, the irradiation data including fission gas release, fission gas retention and swelling are lacking. Reactor physics calculations indicate a strong negative Doppler coefficient for thorium based fuels and generally, negative sodium void coefficients. Loss of flow accidents, with negative void coefficients may take on a very different behavior than conventional systems with mixed oxide fuel.

TABLE OF CONTENTS

LIST OF FIGURES

LIST OF FIGURES (Continued)

LIST OF TABLES

1.0 INTRODUCTION

The transient overpower accident (TOP) is one of two postulated events which are used to examine the response of LMFBR cores to unprotected events. It is postulated to be initiated by a continuous ramp reactivity insertion accompanied by failure to scram. During the review of the Preliminary Safety Analysis Report (PSAR) [1] for the Clinch River Breeder Reactor (CRBR), two generic questions were raised [2]:

1) Is internal fuel motion prior to pin failure, in low ramp rate situations, an important feedback mechanism?

2) What is the effect of flow blockages following pin failure, on the coolability of core?

In addition to these generic safety related questions for LMFBR's, there has been renewed interest in the possibility of using Thorium based fuels in LMFBR's [3]. Such interest naturally leads to the question:

3) What are the safety related implications of using Thorium based fuels in LMFBR's?

This report summarizes the results of studies conducted in support of the U.S. Nuclear Regulatory Commission, Division of Project Management's Technical Assistance Program, and aimed at answering the three questions raised above.

In Chapter 2, the whole core effects of internal fuel pin motion are discussed. The extension of the single pin model used in the JANE code [4] to a multichannel code is presented. Results of calculations for very low burn-up and very high burn-up fuel are presented as a function of initiating ramp rate.

In Chapter 3, core coolability in the presence of fuel plugging following pin failure is addressed. Thermal-hydraulic analysis of the

channel is considered for various configurations including plug porosity, particle diameter, and heat generation rate.

Chapter 4 contains a summary of safety related physics parameters, accident considerations and data required for use with advanced fuels. The discussion is based on a literature review and contains a pertinent reference list.

Each Chapter contains its own conclusions and references.

REFERENCES FOR CHAPTER 1.

1. Preliminary Safety Analysis Report, Clinch River Breeder Reactor, Project Management Corporation, (1975), Docket No. 50-537.

2. V. K. Dhir, et. al. "LMFBR Fuel Analysis Task A: Oxide Fuel Dynamics", NUREG/CR-0011, February 1978.

3. B. R. Sehgal, et.al. "Thorium-Based Fuels in Fast Breeder Reactors," Nuclear Technology, Vol. 35 pp 635-650, October 1977.

4. M. V. Frank, "Some Aspects of Fuel Rod Behavior During a Fast Reactor Overpower Transient", Ph.D. in Engineering, UCLA, December 1978.

2.0 PREFAILURE AXIAL FUEL MOTION

2.1 Introduction

Prefailure axial fuel motion within the central cavity of an LMFBR fuel pin has been described as a potentially important phenomena in transient overpower accidents initiated by mild ramp rates (< 50 cents/sec) [1]. This phenomena had been neglected in existing TOP computer codes (i.e., SAS-3A, MELT II and HOPE). A single pin computer model designated as JANE [2] and formulated at UCLA, does model in-pin axial fuel motion as forced by gravity, fuel thermal expansion, gas bubble addition and expansion in molten fuel. During the past year the JANE code has been extended to multiple channel or whole core capability.

It was shown in the 1977 Task A report [1] that for an input power rise of the form:

$$P = P_o \, e^{t/\tau} \qquad (2.1)$$

where

P_o = initial power and

τ = constant used to simulate a specific ramp rate,

in a single pin, "the potential for significant reactivity change due to axial fuel motion prior to failure increases with decreasing ramp rate and increasing burn-up." However, the actual effect of such prefailure motion can only be investigated within the context of a whole core model. The extension of JANE to treat whole core transients has enabled UCLA to investigate the role of prefailure fuel motion on overall core behavior.

This section begins with a description of the procedure used to develop the whole core JANE model. It is followed by a summary of the development of two data sets which are based on the parameters of the Clinch River Breeder Reactor (CRBR). One set corresponds to high burn-up core, the other

to a low burn-up core. The results of running each of these data sets in JANE, with ramp rates of 1¢/sec 2.4 ¢/sec and 10¢/sec, is presented, and the relative role of fuel motion reactivity prior to failure discussed.

2.2 Whole Core Development

Development of JANE into a whole core model has been carried out under the principle assumption that subassemblies are coupled to each other through reactor power only. Groups of subassemblies with similar power, coolant flow and fuel characteristics are then lumped together and assumed to behave identically as a representative subassembly. An average fuel pin of the subassembly with its associated coolant is used to model the representative subassembly or channel. A number of channels (or representative subassemblies) coupled by the reactor power are used to describe the whole core.

As originally developed, the JANE code follows the steady state and transient behavior of one fuel pin and the thermal characteristics of its associated coolant channel, given the pin power density as a function of time. The addition of kinetics and feedback modules to the code enables one to convert to a whole core model in which only the initial power axial density distribution need be specified.

In JANE, the single fuel pin is divided into 10 radial fuel nodes, 4 radial clad nodes and 10 axial nodes for the fuel and clad. The coolant channel is divided into 35 axial nodes for thermal hydraulics calculations and then averaged into the 10 axial nodes for feedback calculations. The overall core is divided into 8 channels. The multi-channel model is capable of handling as many as 21 axial nodes and as many as 20 channels.

In the kinetics model, the power is assumed to be governed by the point kinetics equations using six delayed groups. These equations are solved using the stabilized forward march technique.[3] The spatial

power shape is assumed constant during the transient.

Feedback effects are calculated for each channel, summed over the whole core and passed to the kinetics module at each time step. At present the code is set up to calculate Doppler, sodium density and fuel motion (pre-failure) feedback.

In the kinetics calculation the core is modelled as a single region. Total reactor power is governed by the lumped parameter kinetics equations:

$$\frac{dP}{dt} = \frac{\rho-\beta}{\Lambda} P + \sum_{i=1}^{6} \lambda_i C_i \qquad (2.2)$$

and

$$\frac{dCi}{dt} = \frac{\beta_i P}{\Lambda} - \lambda_i C_i, \quad i=1,2,\ldots 6 \qquad (2.3)$$

where

ρ = total reactivity

P = total power

C_i = precursor population for group i

λ_i = decay constant for group i

β_i = delayed neutron fraction for group i

β = total delayed neutron fraction

Λ = prompt neutron generation time

The coupled set of equations (2.2) and (2.3) are solved in subroutine KNETICS using a "march-out" algorithm [3]. Once the total power, P(t) at time t is found, the linear power density at node i for channel n is calculated as:

$$LPD(i,n) = \frac{P(t)}{P_o} \times LPDI(i,n) \qquad (2.4)$$

where

LPD(i,n) = linear power density (w/cm)

LPDI(i,n) = initial linear power density (w/cm).

The total reactivity $\rho(t)$ at time t is the sum of the insertion reactivity and the feedback reactivities

$$\rho(t) = \rho_i(t) + \rho_d(t) + \rho_s(t) + \rho_m(t) \qquad (2.5)$$

where

ρ_i = insertion reactivity

ρ_d = Doppler feedback reactivity

ρ_s = sodium density reactivity

ρ_m = fuel motion reactivity

For ramp insertions, the insertion reactivity is a linear function of time:

$$\rho_i(t) = rt \quad \text{(where r is input)}. \qquad (2.6)$$

The Doppler feedback calculation makes use of whole core constants

$$T \frac{d\rho_d}{dt} = -A(i,n) \qquad (2.7)$$

where

A(i,n) = doppler constant for node i of channel n.

The whole core Doppler feedback is given by:

$$\rho_d(t) = \sum_{n=1}^{8} \sum_{i=1}^{10} A(i,n) \ln \left\{ \left[F_m(i,n,t)\, \overline{T}_m(i,n,t) + \left(1 - F_m(i,n,t)\right) \overline{T}(i,n,t) \right] \Big/ \overline{T}_o(i,n) \right\} \qquad (2.8)$$

where

$F_m(i,n,t)$ = fraction of molten fuel at node i of channel n at time t (as determined in Reference [2]).

$\overline{T}_m(i,n,t)$ = average temperature of the molten fuel in node i,

$\overline{T}(i,n,t)$ = average temperature of solid fuel in node i, and

$\overline{T}_o(i,n)$ = initial average temperature of the fuel at node i.

Sodium density reactivity is found using the average sodium density ratio referenced to the hot fuel power density at each node:

$$\rho_s(t) = -\sum_{n=1}^{8}\sum_{i=1}^{10} W_s(i,n)\ \alpha\ (i,n,t) \qquad (2.9)$$

where

$W_s(i,n)$ = reactivity worth of sodium in axial node i and channel n and (this is a negative quantity)

$\alpha(i,n,t)$ = average density ratio of sodium in this segment at time t.

The whole core reactivity due to fuel motion is calculated as follows:

$$\rho_m(t) = \sum_{i=1}^{10}\sum_{n=1}^{8} W_f(i,n)m(i,n,t) - \sum_{i=1}^{10}\sum_{n=1}^{8} W_f(i,n)m_o(i,n) \qquad (2.10)$$

where

$W_f(i,n)$ = worth of fuel per gram at node i in channel n

$m(i,n,t)$ = mass of fuel in node i of channel n at time t

$m_o(i,n)$ = initial mass of fuel in node i channel n.

The above feedback reactivity calculations are carried out in subroutine FEEDBK.

In order to convert the single pin JANE model to a whole core model it was decided not to redimension variables but rather to make use of storage arrays. This gives a more effective and flexible approach to multi-channel conversion, and a substantial savings in cost.

The storage arrays are three vectors in which all of the data that must be saved is stored for a single sample pin in moving from one time step to the next. Each vector is doubly dimensioned. The first dimension gives the location of the single pin parameter being stored while the second dimension is the channel number. A subroutine called CHANL was written and added to the code in order to initialize, update and read these storage arrays.

The storage arrays are first used during the input phase to initialize channel dependent parameters. The subroutine CHANL is called to move data

out of the storage arrays before execution of the steady state and transient one-pin models, at which point single pin parameters are set equal to their values for that channel at the end of the last time step. After the single pin model executes, CHANL is once again called in order to move updated parameters into the storage array so they can be used at the next time step.

A flow chart for the multi-channel JANE code is shown in Figure 2.1.

2.3 Data

In order to demonstrate the operation of the whole core JANE code and the relative effect of fuel motion two data sets were developed. The first set corresponds to the beginning of cycle one (BOC1) and the second to reactor fuel at the end of the cycle one (EOC1). These data sets were based on the CRBRP data originally generated for the HOPE code [4].

The input used in the JANE code describes a liquid metal cooled fast reactor with an equivalent diameter of 188.2 cm divided into two regions, with fuel pins operating at an average power of 216.5 w/cm. The reactor contains 198 hexagonal, canned fuel assemblies each holding 217 fuel pins. The pins are loaded with mixed PuO_2 - UO_2 pellets in the core and depleted UO_2 pellets in the axial and radial blankets. These FFTF type fuel pins are spaced in a 0.726 cm (pitch) triangular array with a 0.142 cm spiral wire rap. Each fuel pin has a cold outer diameter of 0.584 cm and is 291.1 cm in length. The pin is comprised of the bottom end plug, the lower axial blanket (35.56 cm), the core (91.44 cm), the upper axial blanket (35.56 cm), and the top end plug. Each pin is loaded with approximately 153 gm of heavy metal in the core and 63 gm in each axial blanket.

The core is cooled by liquid sodium which flows upward through the core. Thermo-hydraulically, the expected average coolant rise through

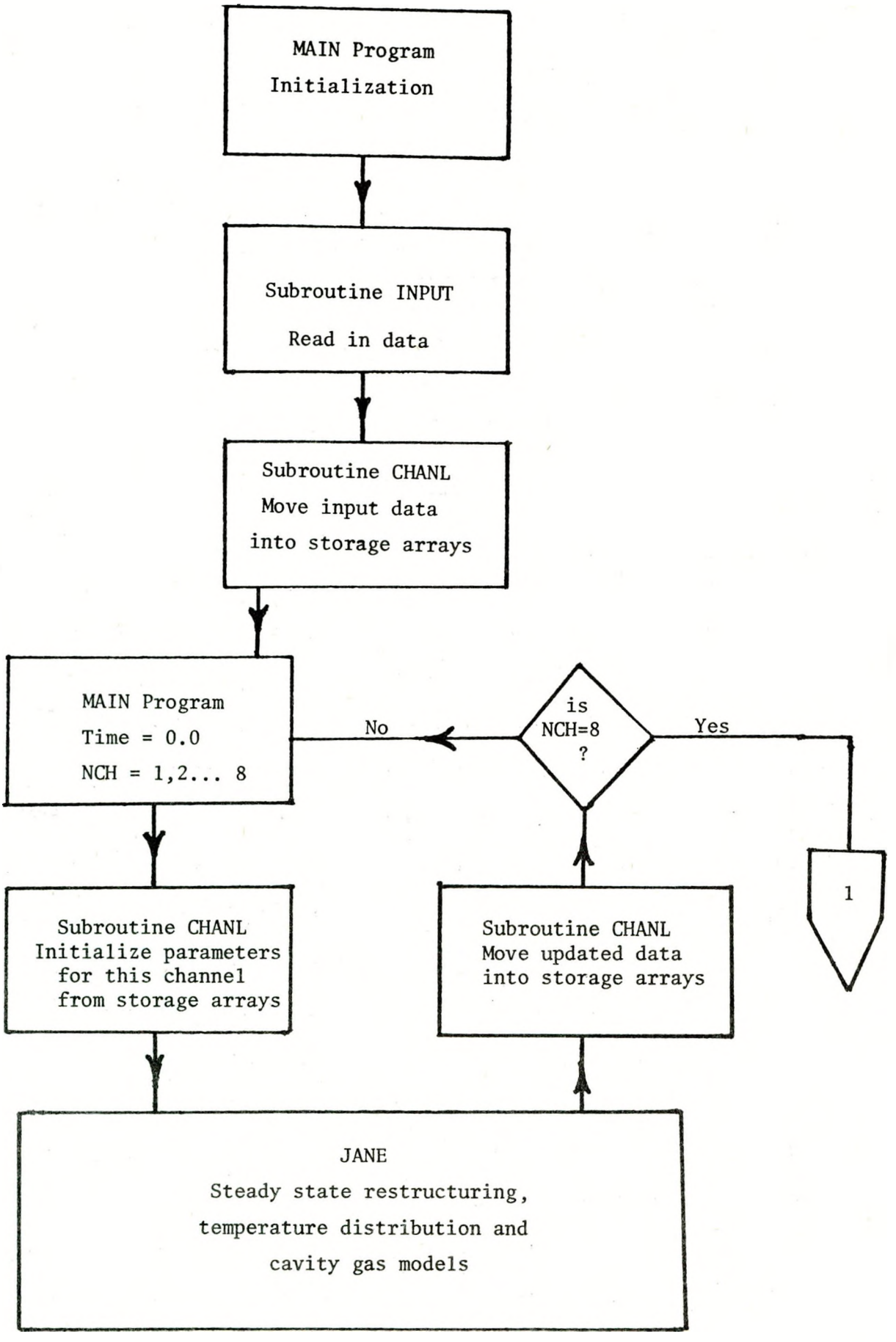

Figure 2.1 Flow Chart of the Whole Core JANE Model.

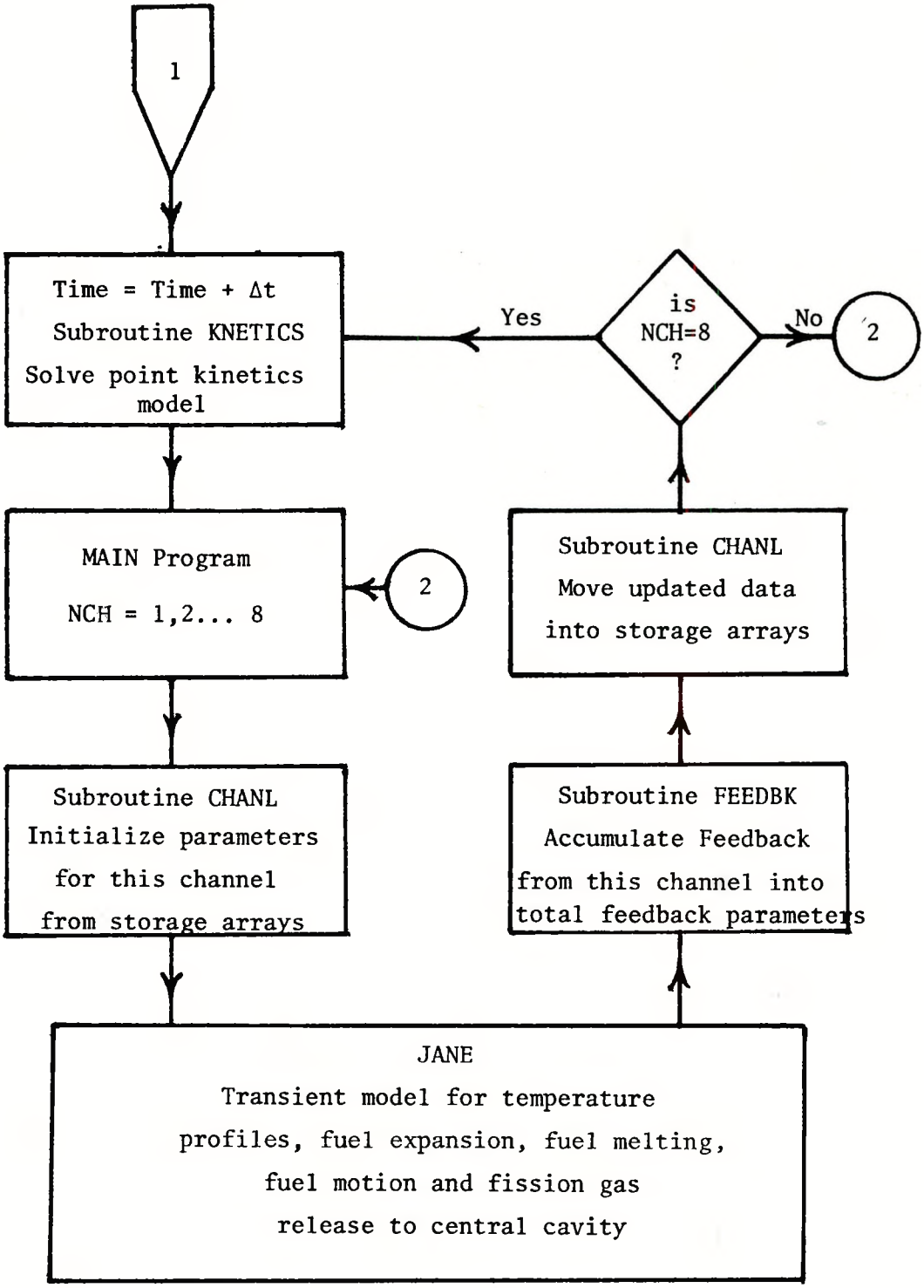

Figure 2.1 (Continued)

the core is 138^{0}C with an inlet sodium temperature of 388^{0}C.

For the JANE runs performed here, the inner and outer core regions were divided into eight channels with six channels representing the inner core and two channels representing the outer core.

Two data sets were compiled in order to carry out the whole core JANE studies. The first of these corresponds to beginning of cycle one (BOC1) fuel which is at 364 megawatt days per metric tonne. This slight burn-up gives the fuel a chance to restructure, otherwise there would be no internal fuel motion because of no cavity. The second data set is based on fuel at the end of cycle one (EOC1) with a uniform burn-up of 80,000 megawatt days per metric tonne. Delayed neutron constants for these two data sets are shown in Table 2.1. Doppler constants and fuel and sodium worths for the two data sets are given by channel in Tables 2.2 and 2.3. The radial and axial power distribution, sodium, fuel and doppler reactivity worths were derived for each axial node of each channel from data sets developed for HOPE runs at UCLA [4] based on CRBRP. The channel representation of the fast reactor core is given in Table 2.4.

2.4 Results

Demonstration of the JANE whole core model was accomplished with six cases. In order to reduce computational time the program was run without the stress-strain calculations. The calculation was stopped when the central cavity of a high power density channel completely filled with molten fuel. A uniform burn-up core is assumed in the six sample cases.

Table 2.1 Delayed Neutron Constants for the Sample JANE Runs

Delayed Neutron Precursor Group (i)	Effective Delayed Neutron Fraction (β_1)	Decay Constant (λ_i) sec^{-1}
First Core (Beginning of Cycle)		
1	8.254×10^{-5}	0.0129
2	7.756×10^{-4}	0.0312
3	6.660×10^{-4}	0.1330
4	1.354×10^{-3}	0.3450
5	5.908×10^{-4}	1.4100
6	1.810×10^{-4}	3.7500
Total β_{eff}	3.650×10^{-3}	
Equilibrium Core (End of Cycle)		
1	8.145×10^{-5}	0.0129
2	7.554×10^{-4}	0.0312
3	6.438×10^{-4}	0.1338
4	1.287×10^{-3}	0.3450
5	5.583×10^{-4}	1.3990
6	1.732×10^{-4}	3.7410
Total β_{eff}	3.50×10^{-3}	

Table 2.2 Sodium Voiding Reactivity and Fuel Worth Per Pin in $ for Each Channel

Channel Number	Sodium Density Reactivity		Fuel Worth	
	BOC1	EOC1	BOC1	EOC1
1	0.218	0.273	.0039	.0029
2	0.335	0.520	.0040	.0028
3	0.304	0.518	.0040	.0029
4	0.383	0.596	.0023	.0019
5	0.601	0.823	.0027	.0022
6	0.611	0.587	.0027	.0025
7	-0.0589	0.253	.0032	.0032
8	-1.108	-0.670	.0020	.0022
Total	1.285	2.90		

Table 2.3 Doppler Constant By Channel *
(Sodium-in Configuration)

Channel Number	Doppler Constant = $T \frac{dk}{dt} \times 10^4$	
	BOC1	EOCI
1	2.77	2.97
2	6.31	5.71
3	7.19	6.30
4	7.80	7.21
5	8.35	10.4
6	5.86	9.61
7	7.46	9.87
8	3.91	5.65
Total	49.65	57.76

*Feedback effect is negative.

Table 2.4 Channel Representation of the Fast Reactor Core

Channel	Coolant Mass Flux (gm/cm^2-sec)	Number of Subassemblies	Mass of Oxide/channel (MT)	Total Fuel Pins
1	557.6	6	0.414	1302
2	557.6	12	0.829	2604
3	557.6	12	0.829	2604
4	518.9	24	1.66	5208
5	502.6	30	2.07	6510
6	437.4	24	1.66	5208
7	518.3	42	2.90	9114
8	383.1	48	3.32	10416

Three of the cases were for high burn-up fuel, the other three for low burn-up. The matrix of cases is summarized in Table 2.5. Input parameters for the sample cases are given in Table 2.6.

Power and reactivity histories for the six sample cases are given in Figures 2.2 to 2.13. There are two figures for each case. The first figure displays the overall power and reactivity versus time from the beginning of the transient until program termination (as described above). The second figure in each set gives the same information but starting from the time when fuel motion begins to contribute reactivity as a flowing slug or plug in the central cavity of the fuel pins. In each figure the power factor $(P(t)/P_o)$ is given as a dotted line and read on the right y axis. Reactivity is on the left y axis. The three principle feedback reactivities - fuel motion, sodium and Doppler - along with total reactivity are given. Total reactivity includes the ramp insertion reactivity.

One sees from these figures that prior to failure, Doppler is the major feedback reactivity and is negative. The positive sodium feedback is an order of magnitude smaller than the Doppler before failure.

The JANE fuel motion model predicts viscous damped, gravity driven slug flow for the sample cases. Therefore, the initial fuel motion is downward, initiating above the midplane. If the slug reaches the bottom of the central cavity, it will begin to backfill with molten fuel. The downward flowing molten fuel and increasing molten fuel inventory in the bottom half of the core causes an increased energy deposition in the bottom half of the core. This causes the peak fuel temperature to relocate below the core midplane from its pretransient position above the midplane. Thus more fuel melts and slumps toward the bottom half of the fuel pin than would be expected by a symmetric axial energy deposition.

Table 2.5 JANE Whole Core Case Matrix

Burn-up (MWD/MT)	Ramp Rate		
	10¢/sec	2.4¢/sec	1.0 ¢/sec
364	B1	B2	B3
80000	E1	E2	E3

Table 2.6 Input Parameters for the Sample Cases

Burn-up (MWD/MT)		Columnar Grain* Zone Transition Temperature °C		Equiaxed Grain* Zone Transition Temperature °C	
BOC1	EOC1	BOC1	EOC1	BOC1	EOC1
364	80000	1889.0	1517.4	1586.0	1329.7

Fuel Radial Nuclear Peaking Factors

Channel #	1	2	3	4	5	6	7	8
BOC1	1.114	1.181	1.171	1.105	0.995	0.900	1.070	0.837
EOC1	1.215	1.040	1.130	1.027	1.018	0.923	1.101	0.871

Peak Linear Power Density (w/cm)

BOC1	312.0	337.3	335.8	316.3	282.5	254.5	306.5	240.8
EOC1	298.2	255.5	278.7	255.7	253.7	232.7	276.0	219.2

*CRBR-PSAR Appendix D.

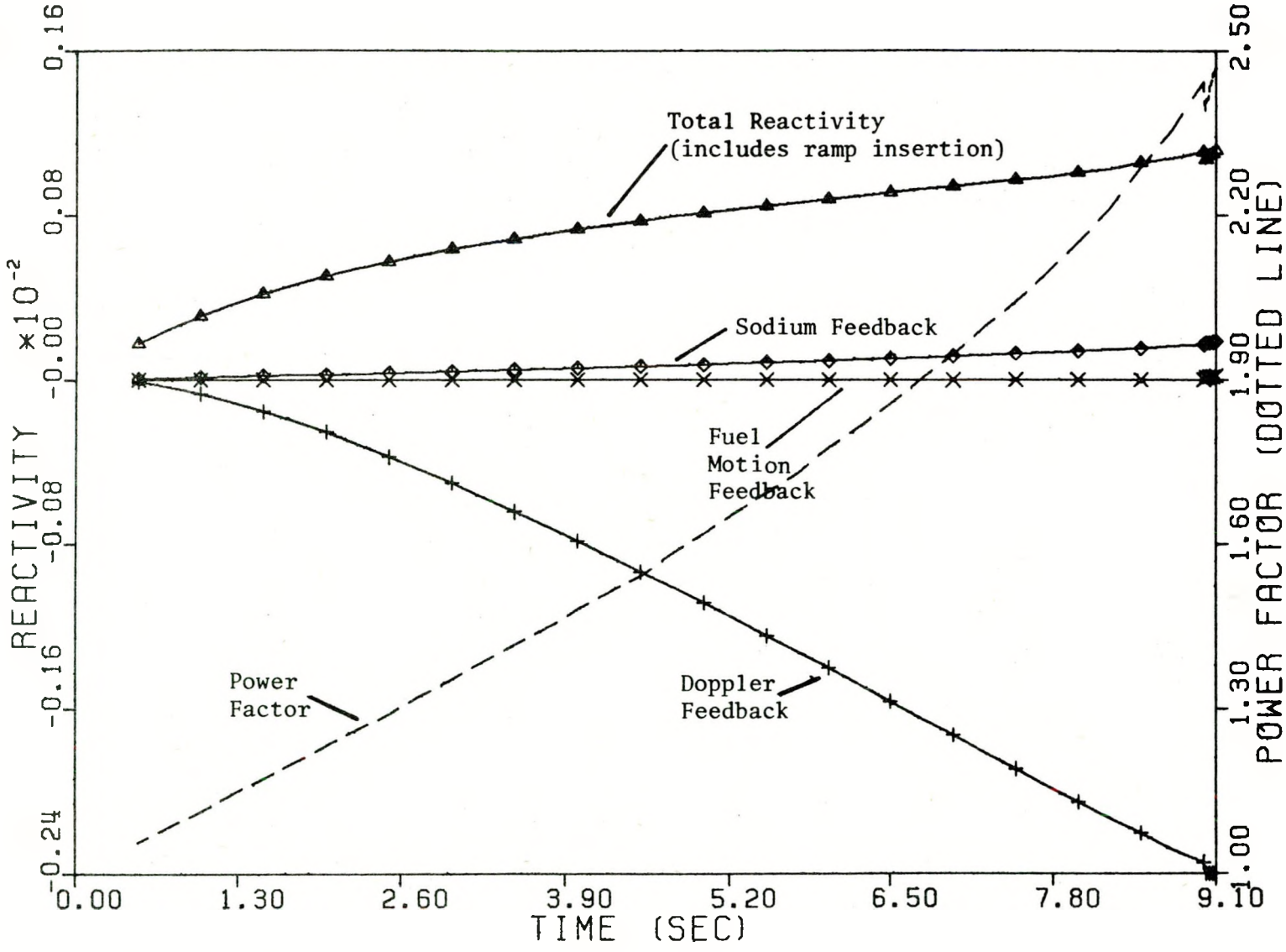

Figure 2.2 BOC1 Power and Reactivity Versus Time
For Case B1.

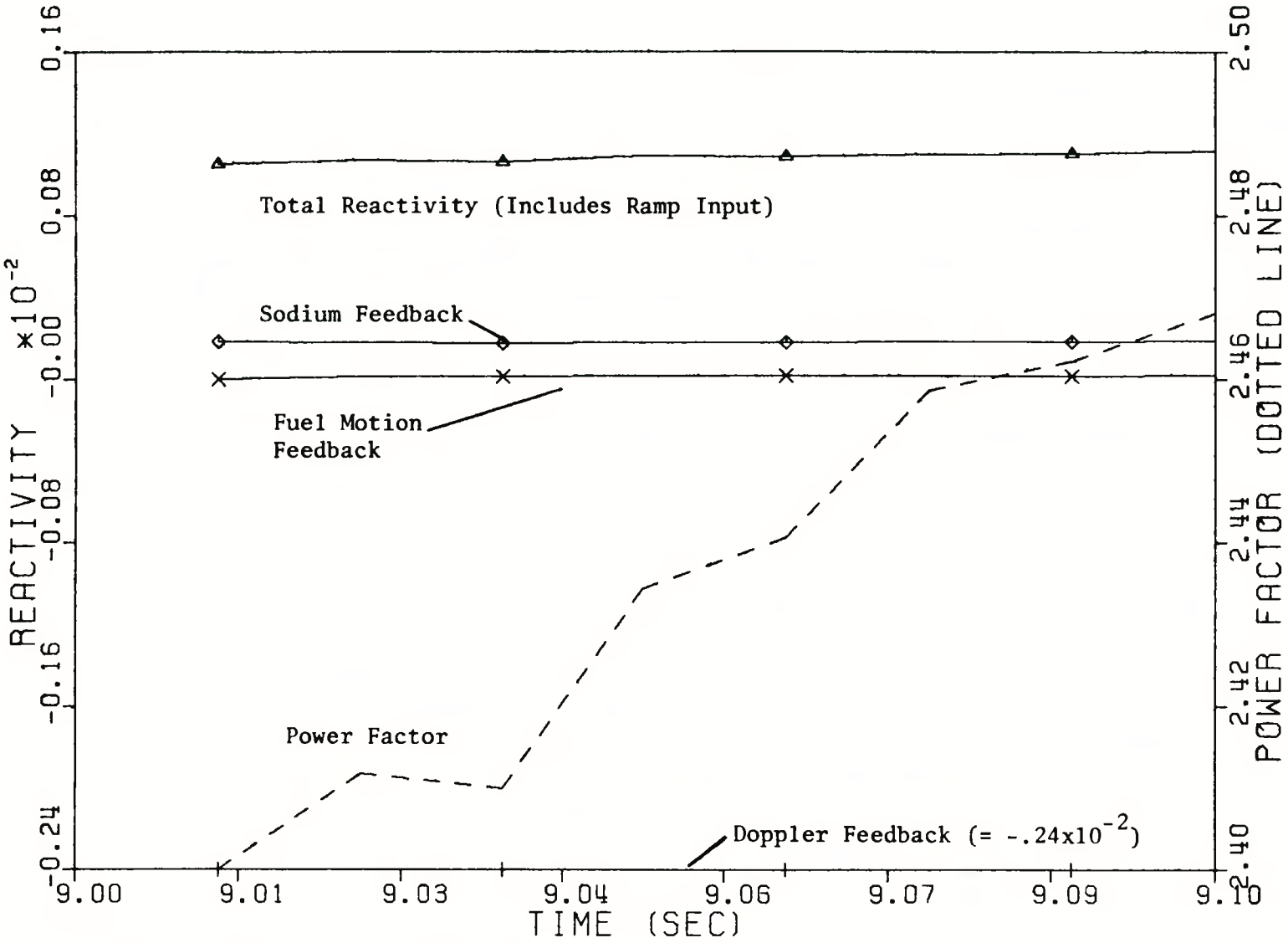

Figure 2.3 BOC1 Power and Reactivity Versus Time after Fuel Motion Begins For Case B1.

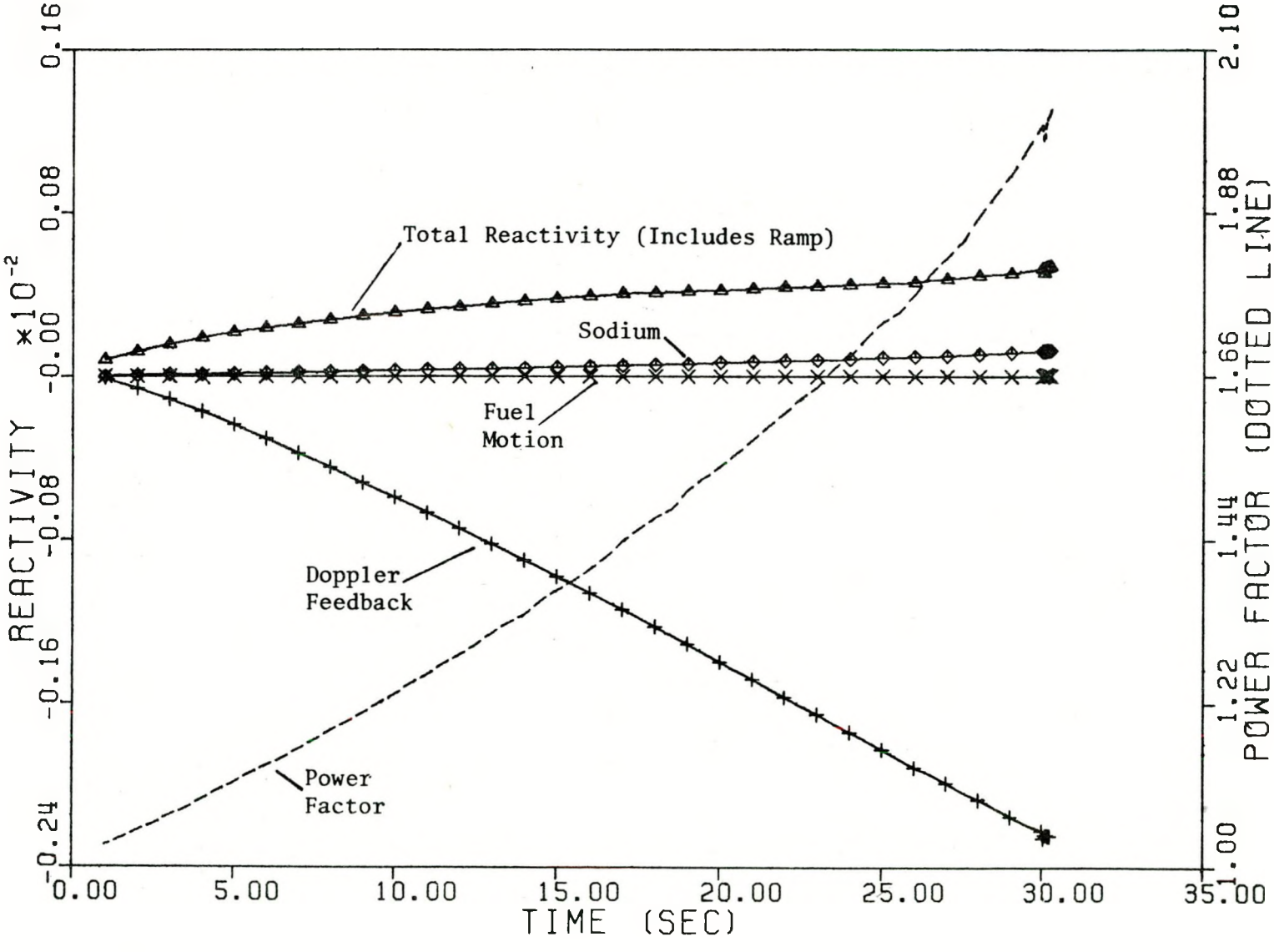

Figure 2.4 BOC1 Power and Reactivity Versus Time For Case B2.

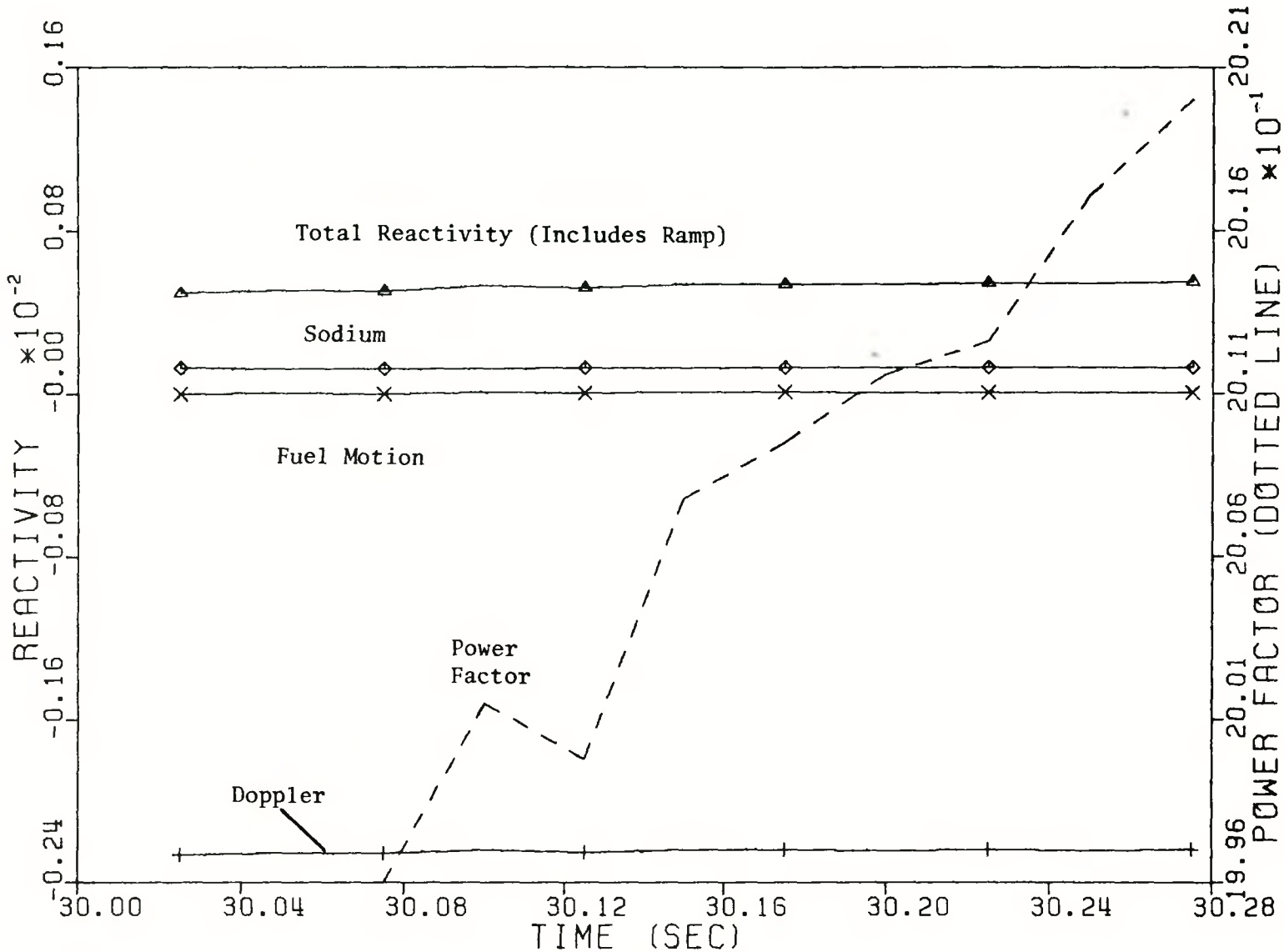

Figure 2.5 BOC1 Power and Reactivity Versus Time After Fuel Motion Begins For Case B2.

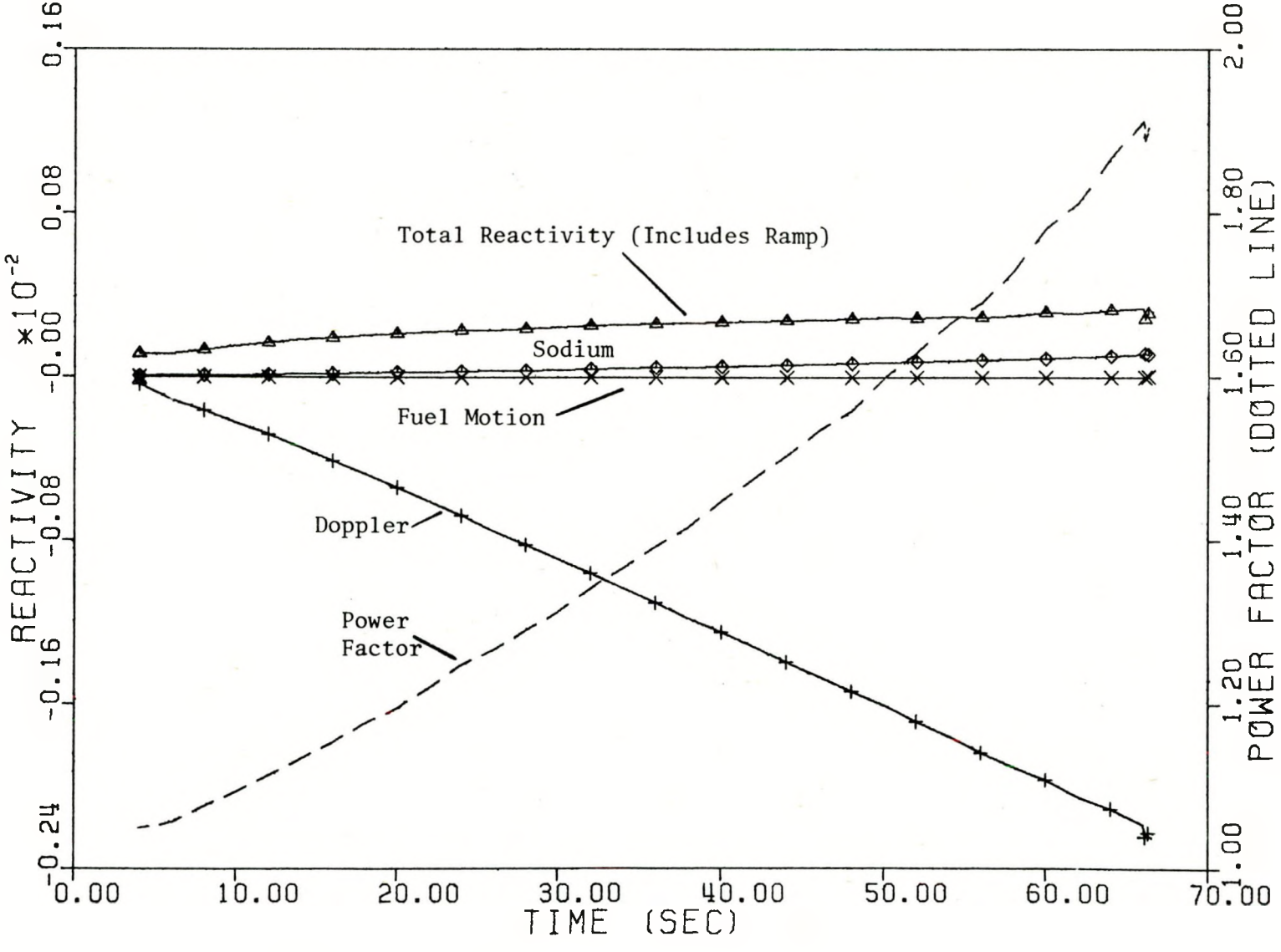

Figure 2.6 BOC1 Power and Reactivity Versus Time For Case B3.

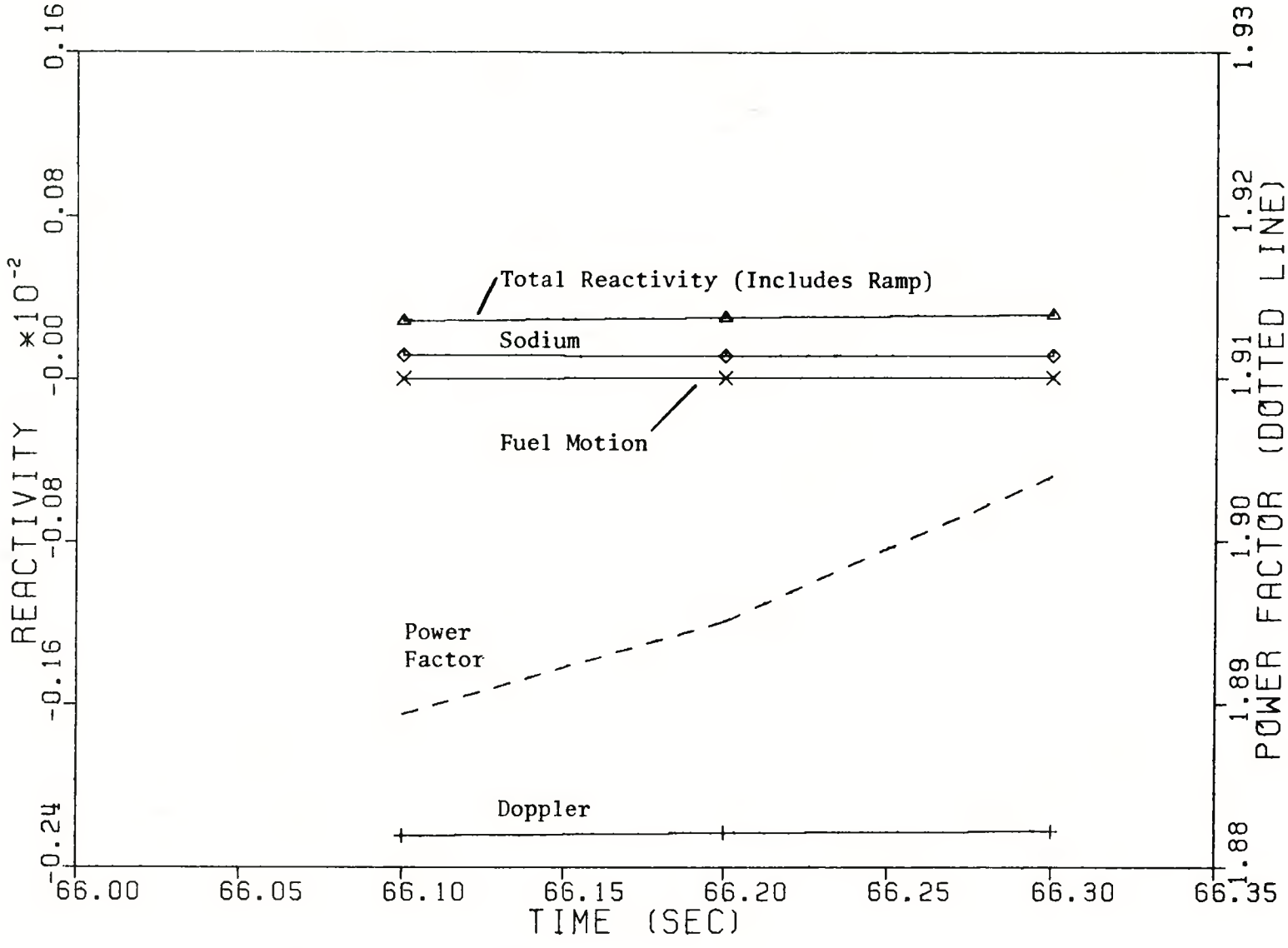

Figure 2.7 BOC1 Power and Reactivity Versus Time After Fuel Motion Begins for Case B3.

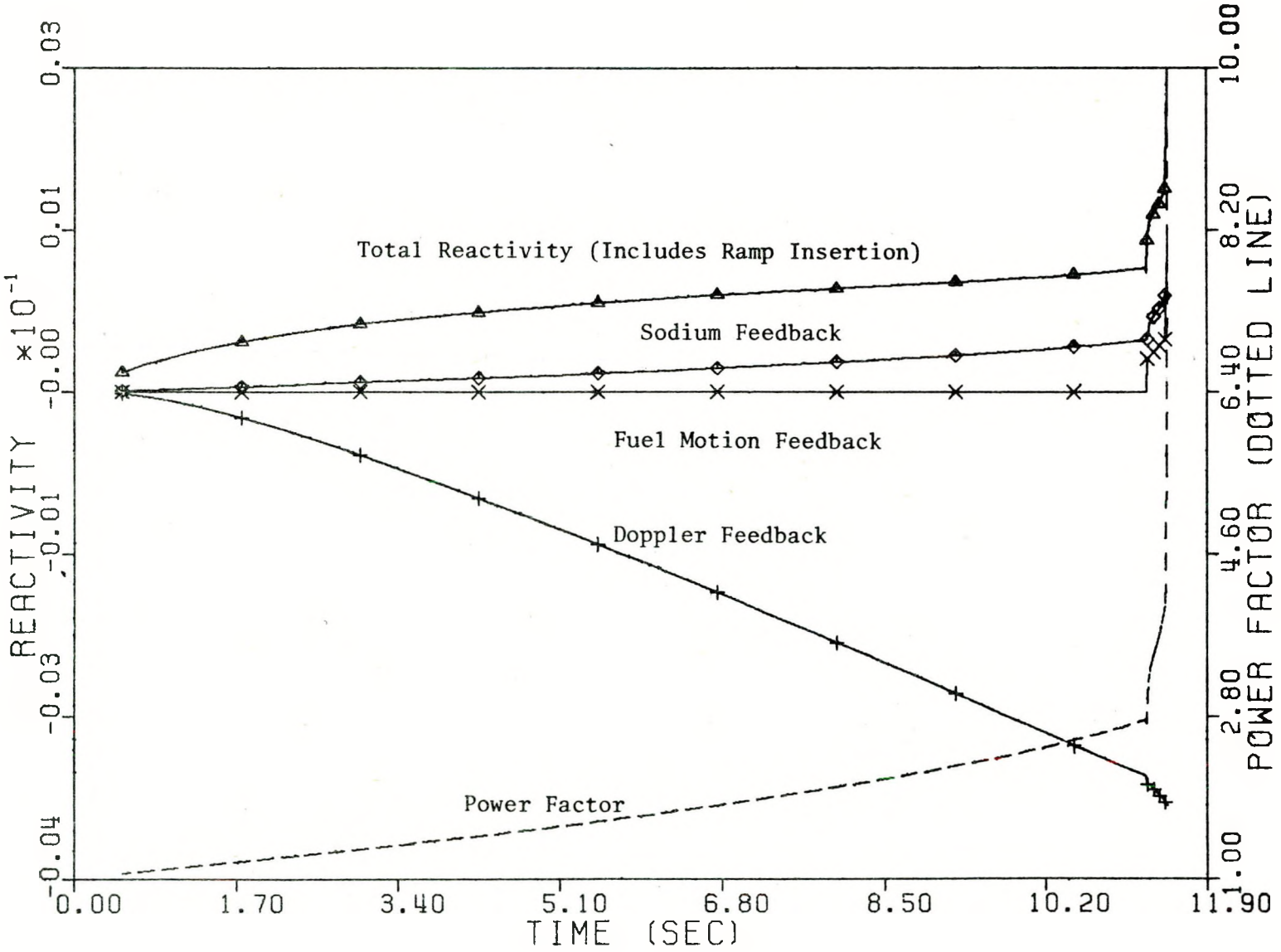

Figure 2.8 EOC1 Power and Reactivity Versus Time For Case E1.

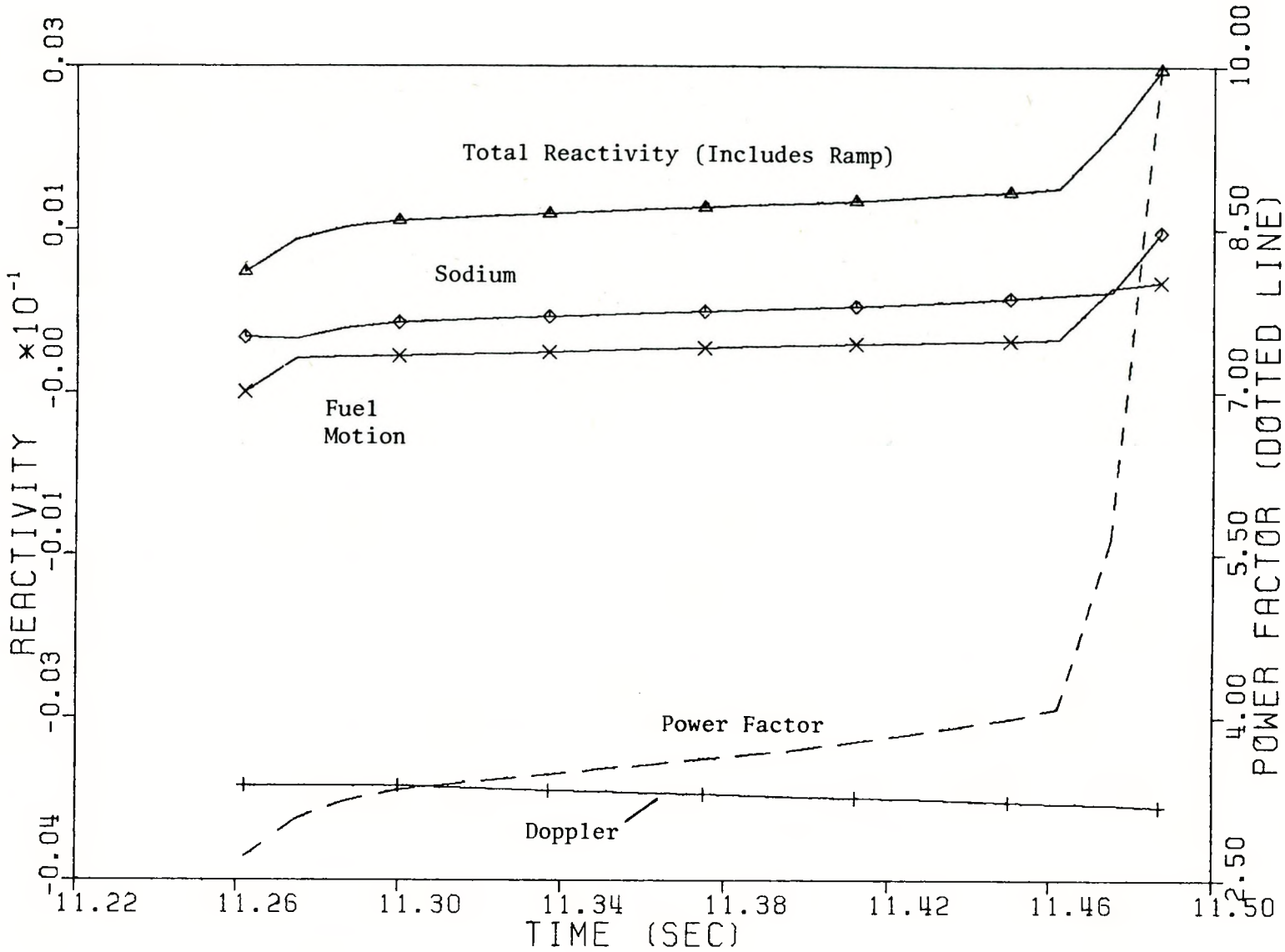

Figure 2.9 EOC1 Power and Reactivity Versus Time After Fuel Motion Begins For Case E1.

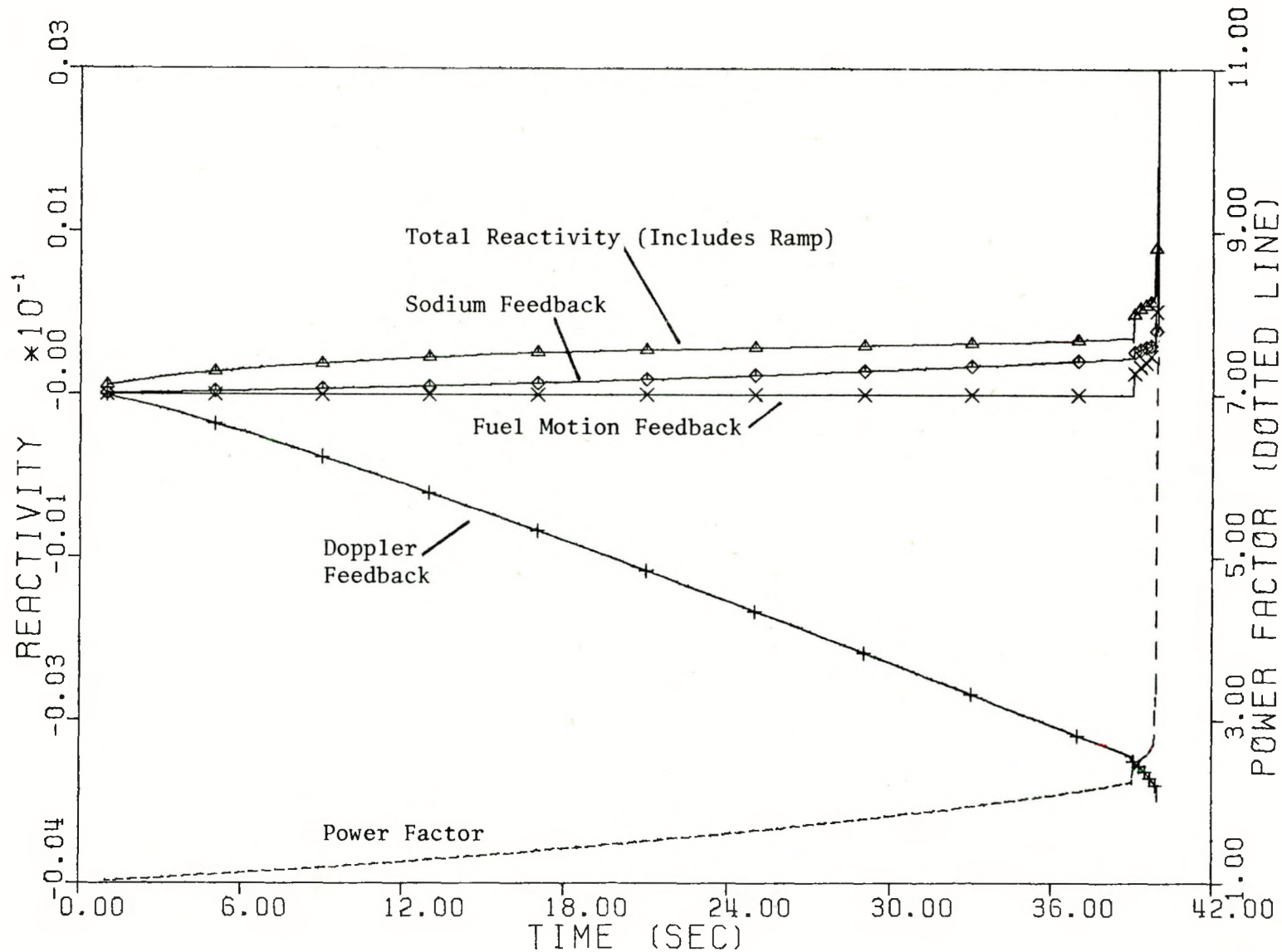

Figure 2.10 EOC1 Power and Reactivity Versus Time

For Case E2.

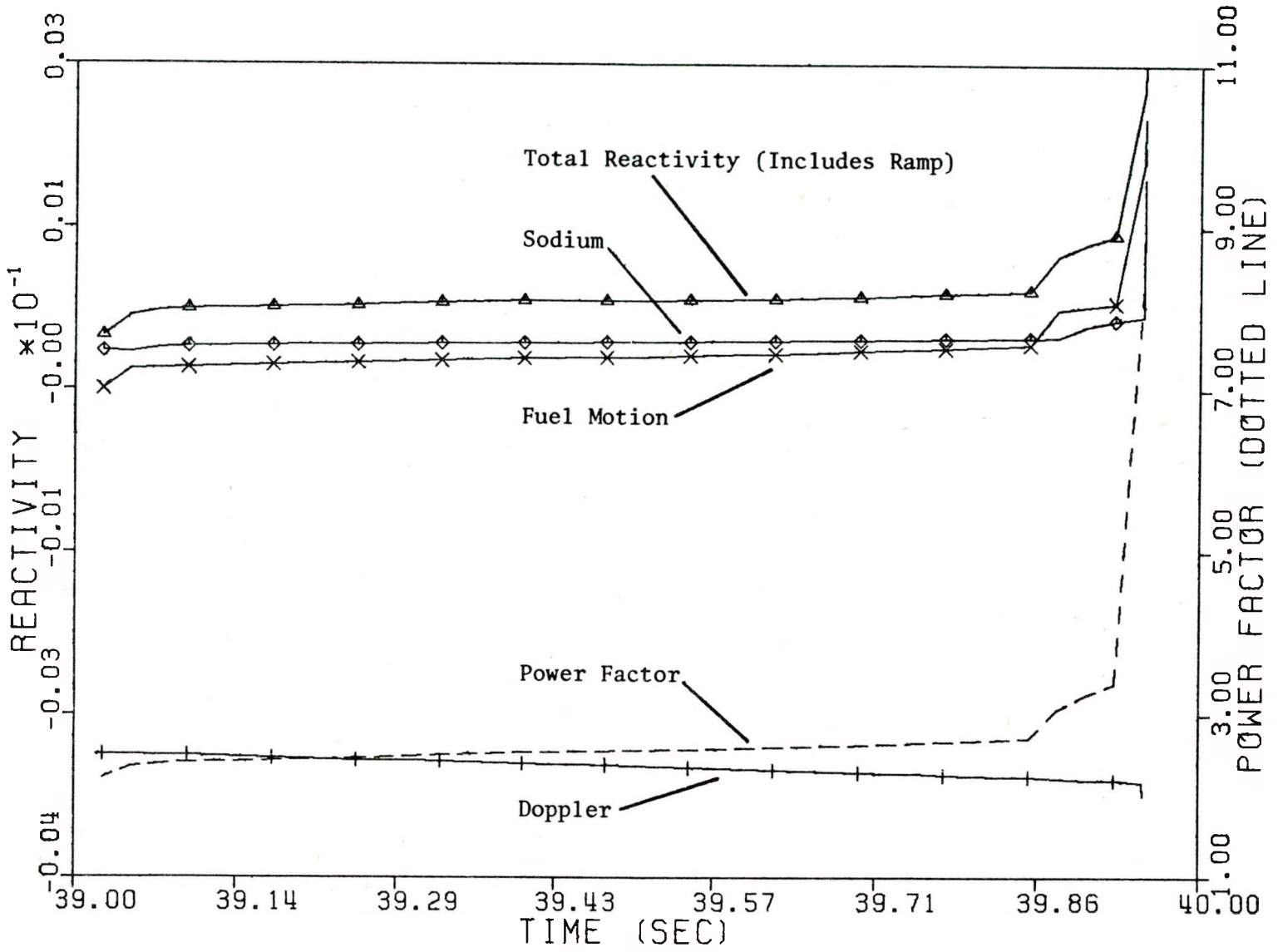

Figure 2.11 EOC1 Power and Reactivity Versus Time After Fuel Motion Begins for Case E2.

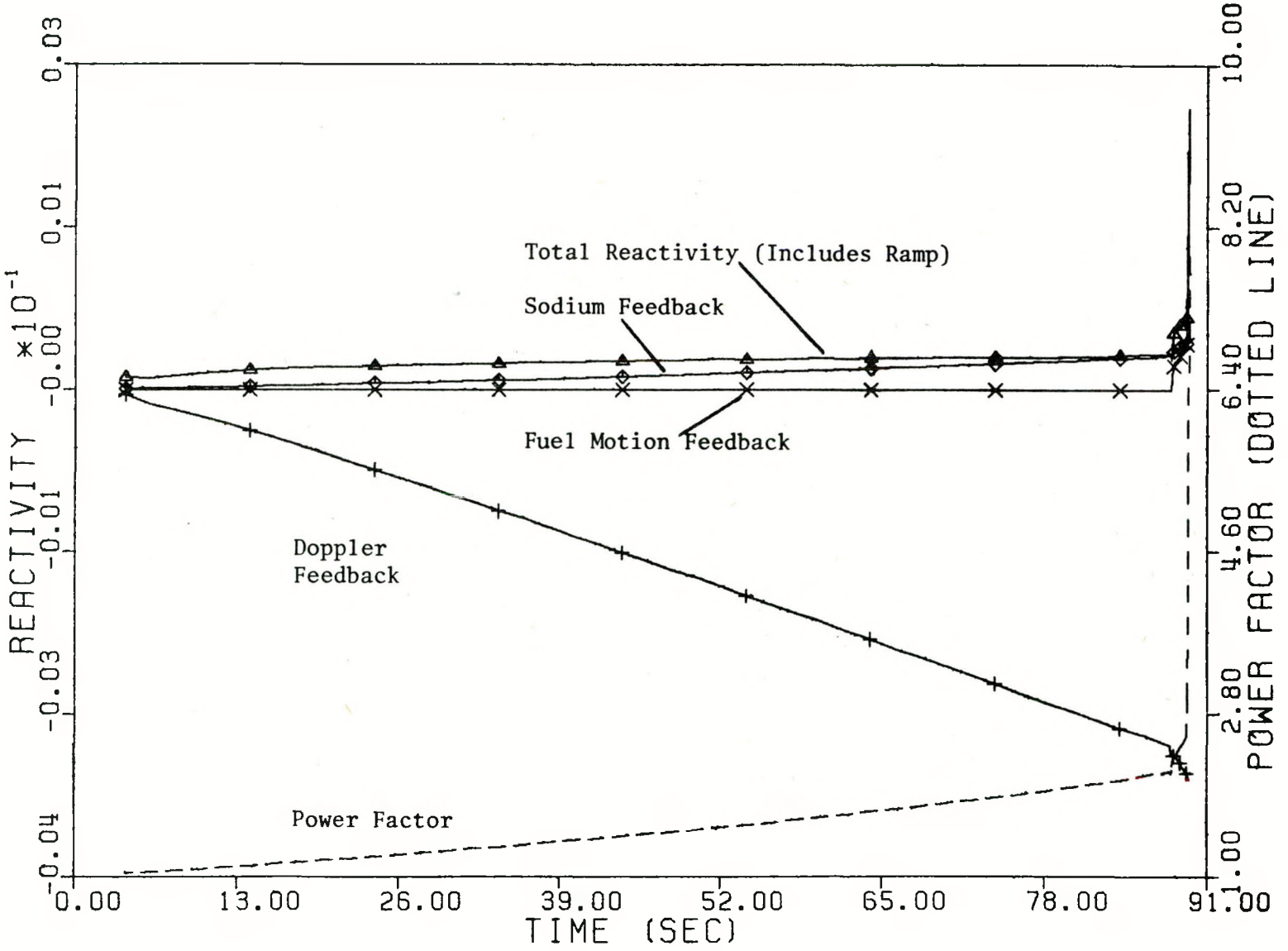

Figure 2.12 EOC1 Power and Reactivity Versus Time For Case E3.

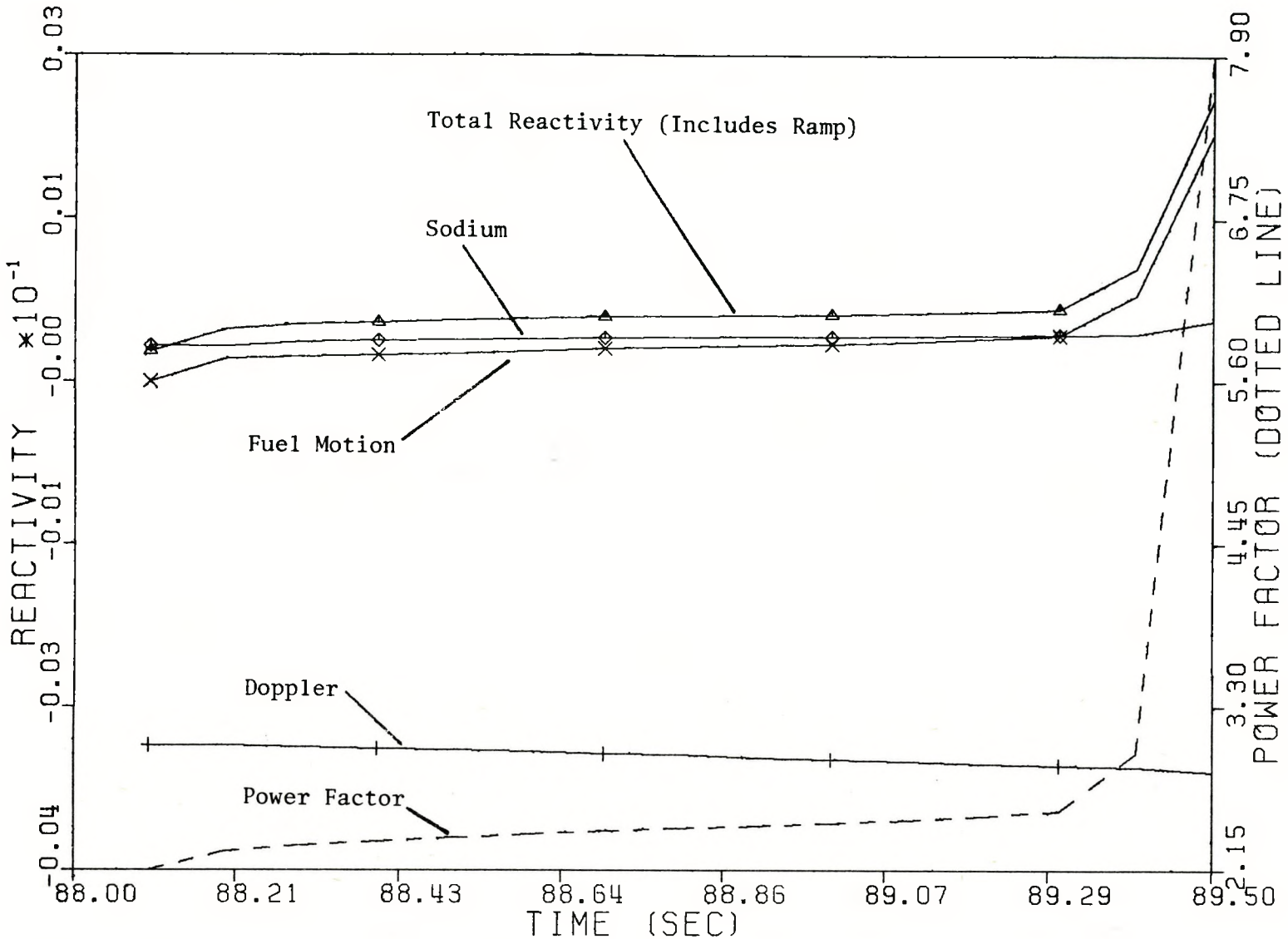

Figure 2.13 EOC1 Power and Reactivity Versus Time After Fuel Motion Begins For Case E3.

The result is a net redistribution of fuel toward the bottom half of the fuel pin. The integral fuel worth below the core midplane is larger than above the core midplane for CRBR. (The effect seems to be more apparent at BOC1 than EOC1). Therefore, the fuel motion feedback is always positive for the six sample cases.

In the BOCI case fuel motion reactivity is rather insignificant and contributes about an order of magnitude less reactivity than the sodium density feedback. In the EOC1 core the fuel motion feedback is much more important. In all of the EOC1 cases, fuel motion reactivity rapidly grows and takes on the same order of magnitude as the Doppler feedback, but with an opposite sign. This indicates that there may be more potential for significant fuel motion feedback effects at high burn-up as compared with low burn-up. However, an important consideration is that high burn-up fuel is much more likely to fail early in the transient, when compared to low burn-up fuel.

A summary of fuel motion results from the six cases is given in Tables 2.7 to 2.12. Figures 2.4 to 2.18 give graphic description of some of the more significant fuel motion described in Table 2.7 to 2.12.

2.5 Discussion

Based on the results presented, it appears that for the EOCI (high burn-up) core, fuel motion can potentially cause a much larger positive reactivity effect than it can for the BOCI (low burn-up) case. For the BOCI core, prefailure fuel motion introduces a very small positive reactivity effect as can be seen in Figures 2.2 to 2.8. In all of the BOC1 cases, the fuel motion reactivity was at least two orders of magnitude smaller than Doppler feedback at the time of termination. The largest low burn-up fuel motion feedback came from the 1¢/sec ramp (case B-3) with a total fuel motion reactivity of +0.47 cents compared to a Doppler feedback of -66.0 cents and a sodium void feedback of +5.1 cents at the time of termination.

The EOC1 core has prefailure fuel motion which results in a much larger positive reactivity feedback. This can be seen in Figures 2.9 to 2.14. In all

of the EOC1 cases the fuel motion reactivity was of the same order of magnitude as the Doppler feedback, but of opposite sign of the time of program termination. Largest fuel motion feedback came from the 2¢/sec ramp (case E2) with a fuel motion reactivity of 61 cents compared to a Doppler feedback of -96 cents and sodium void feedback of 15 cents at time of termination.

In general, the significance of prefailure fuel motion is expected to increase with decreasing ramp rate. A large ramp rate which yields a very fast heat-up and radial fuel expansion would cause cladding failure prior to substantial axial fuel displacement in the central cavity. Inspection of Tables 2.11 to 2.13 and Figures 2.17 to 2.19 shows that an average flowing fuel velocity over the 150 mm to the cavity bottom is about 100 mm/sec. Therefore, fuel flow progresses for a maximum of one to two seconds, This is a short time compared to the time to failure of a TOP with ramp rates less than 10¢/sec but a long time for transients initiated by ramp rates greater than $1/sec. However, the criterion chosen for run termination (filling of the central cavity with molten fuel) caused an apparent discrepancy between the results and the expectation. The very low ramp rate of 1¢/sec allowed time for the fuel in channels 1 and 7 to reach the cavity bottom and begin backfilling prior to run termination. When this occurs, JANE sets the downward flow velocity to zero. Since backfill has the same reactivity effect as a flow of fuel toward the midplane, the net positive fuel motion reactivity was somewhat diminished in case E3. Since case E2 had a higher ramp rate, it filled the hottest cavity while all fuel flow was downward. Had this case continued, a similar effect would have been observed.

The effect of burn-up on the prefailure fuel motion reactivity results can be explained by considering the following factors:

1) As burn-up increases, the temperature at which fuel restructures decreases. Thus the calculated central cavity size increases. Because of surface tension forces, the onset of fuel motion is

delayed until the surface is broken by the creation of a slug across the diameter of the central cavity [2]. Therefore, at higher burn-up more fuel in each rod may move simultaneously. Furthermore, since the velocity of motion is proportional to the square of the cavity radius [2], the downward flow velocity increases with burn-up.

2) At EOC1 the fraction of power generated in the core is substantially less than at BOC1. This results in reducing the peak linear power densities in the hot channels by approximately 10 to 20 percent. The effect of the reduced power density is similar to reducing the ramp rate.

3) A significant shift in the radial power profile occurs between BOC1 and EOC1 as shown in Reference 4. The normalized power in channels 2 through 4 becomes relatively smaller to that of channels 7 and 8 which becomes relatively larger.

This last factor is a significant contributor in explaining the dramatic difference in calculated fuel motion reactivity between the BOC1 and EOC1 cases. The hottest three channels in the BOC1 cases are 1, 2 and 3. These are representative of 6510 as modeled in JANE (Table 2.5). The hottest three channels in the EOC1 cases are 1, 3 and 7 which represent 13,020 pins. Comparison of Figures 2.9 to 2.13 with Tables 2.11 to 2.13 show that a very large and rapid positive reactivity by insertion (at least 50¢) occurs whenever fuel motion initiates in channel 7 for each EOC1 case. Since 9114 fuel pins are represented by channel 7, this reactivity insertion occurs because

fuel motion is modeled as occurring simultaneously over a large fraction of the core. In contrast, only 5,208 fuel pins are involved with fuel motion during the BOC1 cases.

The results presented in this report are considered to be a conservative (more positive pre-failure fuel motion feedback than expected) estimate. There are three reasons for the conservation.

A) The molten fuel was allowed to flow to the central cavity bottom unimpeded by a potential pressure increase owing to the compression of the cavity gas below the slug. If this gas cannot flow through or around the molten fuel slug, then flow would be expected to stop when

$$\rho_f V_f g = \frac{N_g R T_g}{V_g} Ac \qquad (2.11)$$

where

$\rho_f V_f$ = the mass of flowing fuel in the central cavity,

$\frac{N_g R T_g}{Vg}$ = the pressure of fission gas (ideal gas law) below the slug, and

Ac = the cross sectional area of the central cavity elevation that the flow stops.

The elevation at which this condition is satisfied would be higher than the cavity bottom. This consideration is moot if fuel flows as a film and not a slug.

B) It is not expected that all the pins in Channel 7 would act coherently. Use of more channels would reduce the large simultaneity effect of fuel motion discussed above,

C) It should be recalled that the runs terminated when a central cavity was calculated to fill with molten fuel. The cavity pressure of the hottest channels at this time was far in excess of those expected to produce cladding failure, A more physically reasonable termination criterion based on cladding failure may be expected to reduce the pre-failure fuel motion reactivity feedback for those channels. However, other cooler channels may experience pre-failure fuel motion after the failure of the hottest channels. Therefore, a more meaningful evaluation would include the fuel motion incoherency effects of delayed failure in the cooler channels. The JANE code may be utilized for this further study.

Future work may include evaluation of the effect of equation 2.11 in limiting axial fuel motion, increasing the number of channels used to represent the core, and basing run termination on the failure prediction, stress-strain modeling of the JANE code.

Table 2.7 Fuel Motion Results for Case B1

Channel	Time of Incipient Melting (sec)	Time of Flow Initiation	Time of Flow Termination	Plug or Layer Flow	Average Flow Velocity (cm/s)
2	7.25	9.025	9.100**	Plug	3.888
3*	7.25	9.000	9.0125	Plug	0.0
1	7.75	No Flow			
4	7.75	" "			
7	8.00	" "			
5	8.75	" "			

* Channel which caused program termination

** Flow did not terminate before the end of the program at 9.10 s.

Table 2.8 Fuel Motion Results for Case B2

Channel	Time of Incipient Melting (sec)	Time of Flow Initiation	Time of Flow Termination	Plug or Layer Flow	Average Flow Velocity (cm/s)
2	24.00	30.000	30.275**	Plug	0.775
3*	24.00	30.050	30.125	Plug	16.47
4	26.00	No Flow			
1	26.50	" "			
7	27.00	" "			
5	29.50	" "			

* Channel which caused program termination

** Flow did not terminate before the end of the program at 30.275 s.

Table 2.9 Fuel Motion Results For Case B3

Channel	Time of Incipient Melting (sec)	Time of Flow Initiation	Time of Flow Termination	Plug or Layer Flow	Average Flow Velocity (cm/s)
2	52.00	66.00	66.30	Plug	0.630
3*	52.00	66.10	66.20	Plug	0.0
1	58.00	No Flow			
4	58.00	" "			
7	60.00	" "			
5	66.00	" "			

* Channel which caused program termination

** Flow did not terminate before the end of the program at 66.30 sec.

Table 2.10 Fuel Motion Results For Case E1

Channel	Time of Incipient Melting (sec)	Time of Flow Initiation	Time of Flow Termination	Plug or Layer Flow	Average Flow Velocity (cm/s)
1	9.25	11.250	11.487	Plug	10.929
3*	9.75	11.450	11.487**	Plug	0.793
7	10.00	11.475	11.487	Plug	0.0
4	10.50	No Flow			
2	10.75	" "			
5	10.75	" "			
6	11.25	" "			
8	11.44	" "			

* Channel which caused program termination.

** Flow did not terminate before the end of the program at 11.4875 s.

Table 2.11 Fuel Motion Results for Case E2

Channel	Time of Incipient Melting (sec)	Time of Flow Initiation	Time of Flow Termination	Plug or Layer Flow	Average Flow Velocity (cm/s)
1*	32.5	39.00	39.95**	Plug	10.93
3	35.0	39.825	39.95**	Plug	0.793
7	35.0	39.90	39.95**	Plug	19.32
2	38.0	No Flow			
4	38.0	" "			
5	38.0	" "			
6	39.675	" "			
8	39.95	" "			

* Channel which caused program termination

** Flow did not terminate before the end of the program at 39.95 s.

Table 2.12 Fuel Motion Results For Case E3

Channel	Time of Incipient Melting (sec)	Time of Flow Initiation	Time of Flow Termination	Plug or Layer Flow	Average Flow Velocity (cm/s)
1*	72.00	88.00	89.30	Plug	7.911
3	78.00	89.20	89.50**	Plug	0.920
7	80.00	89.30	89.50	Plug	15.362
2	86.00	No Flow			
4	86.00	" "			
5	86.00	" "			
6	89.00	" "			
8	89.50	" "			

* Channel which caused termination

** Flow did not terminate before the end of the program at 89.50 s.

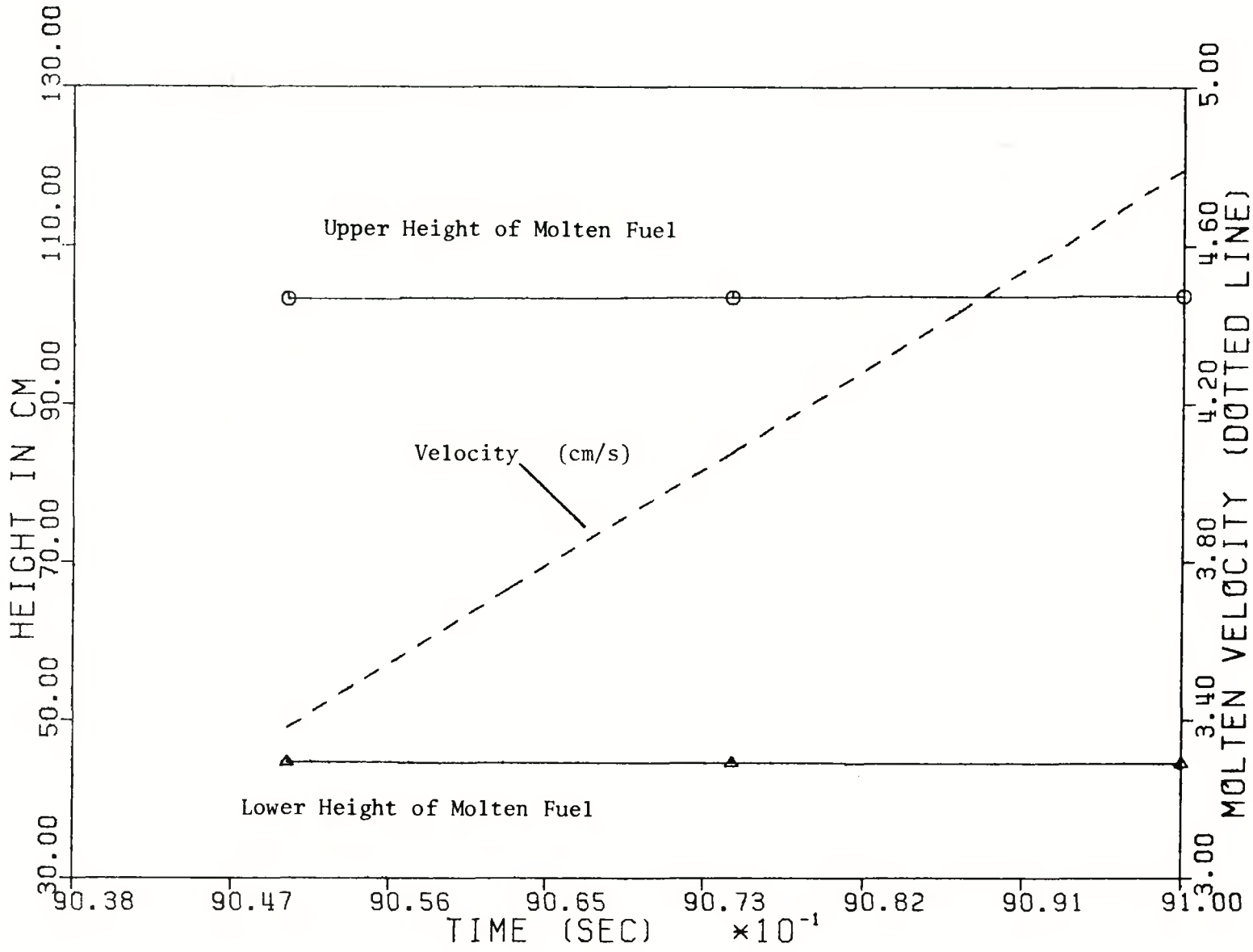

Figure 2.14 BOCl Molten Fuel Height and Velocity
For Channel 2 of Case B1

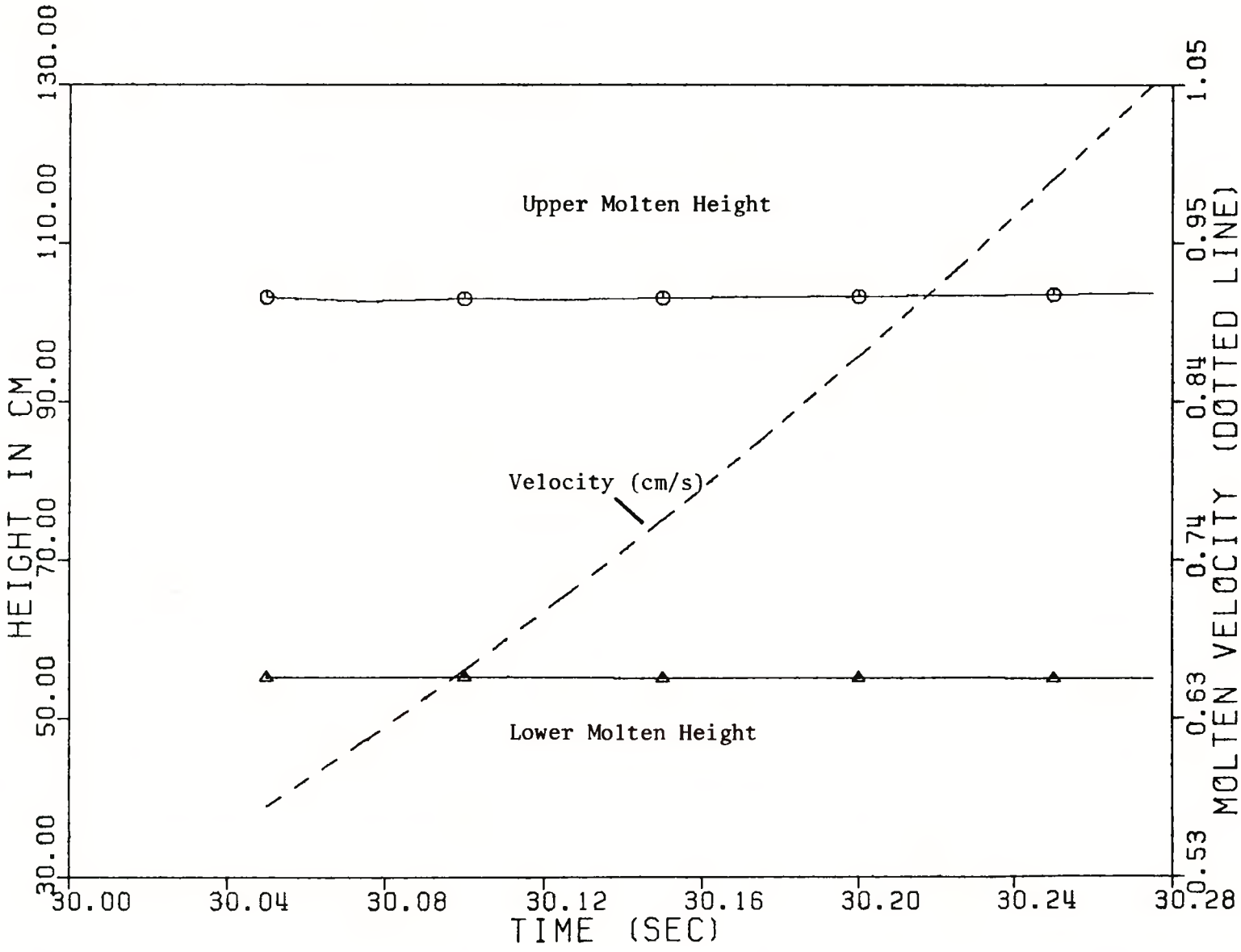

Figure 2.15 BOC1 Molten Fuel Height and Velocity
For Channel 2 of Case B2.

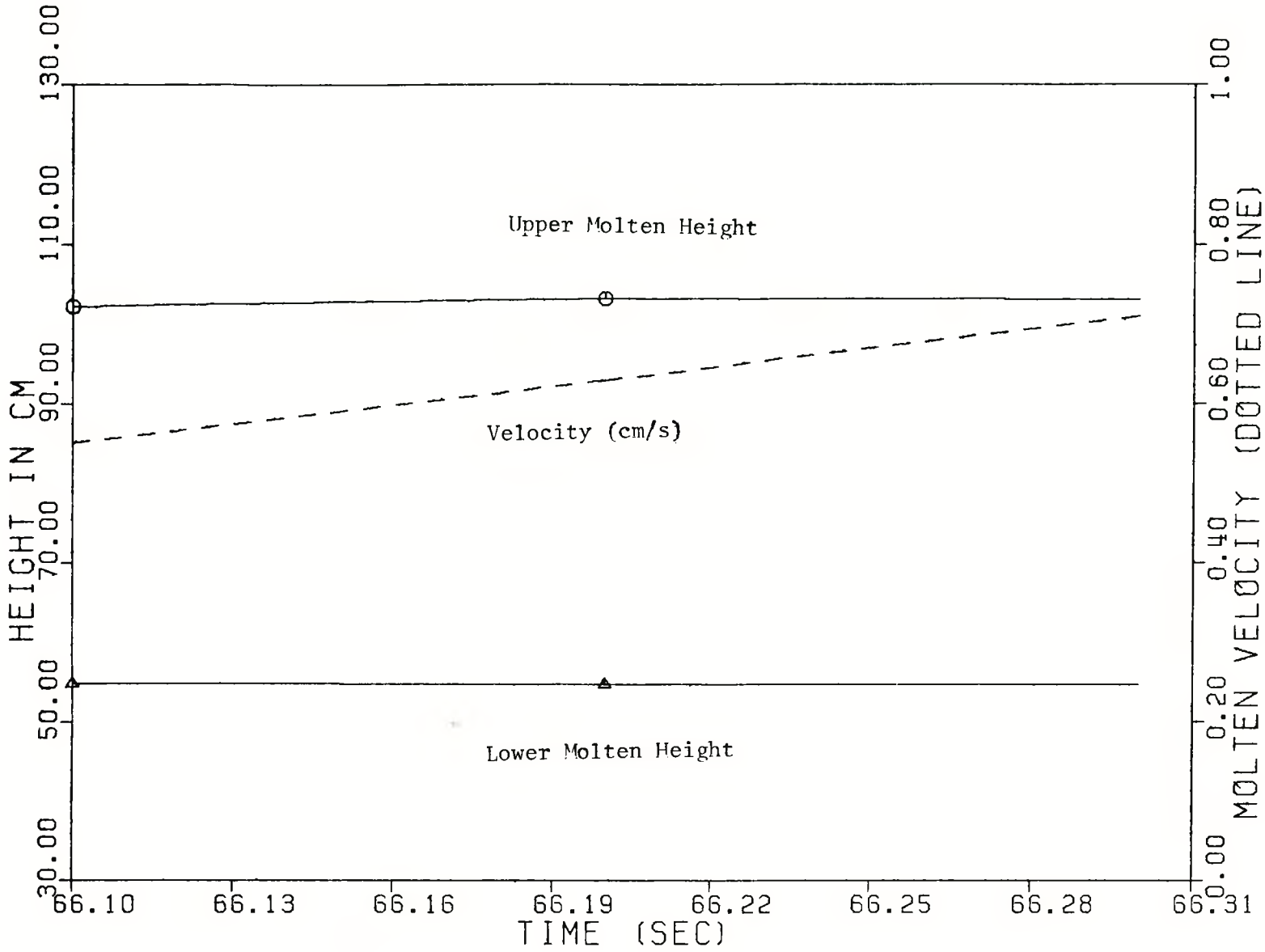

Figure 2.16 BOCl Molten Fuel Height and Velocity
For Channel 2 of Case B3

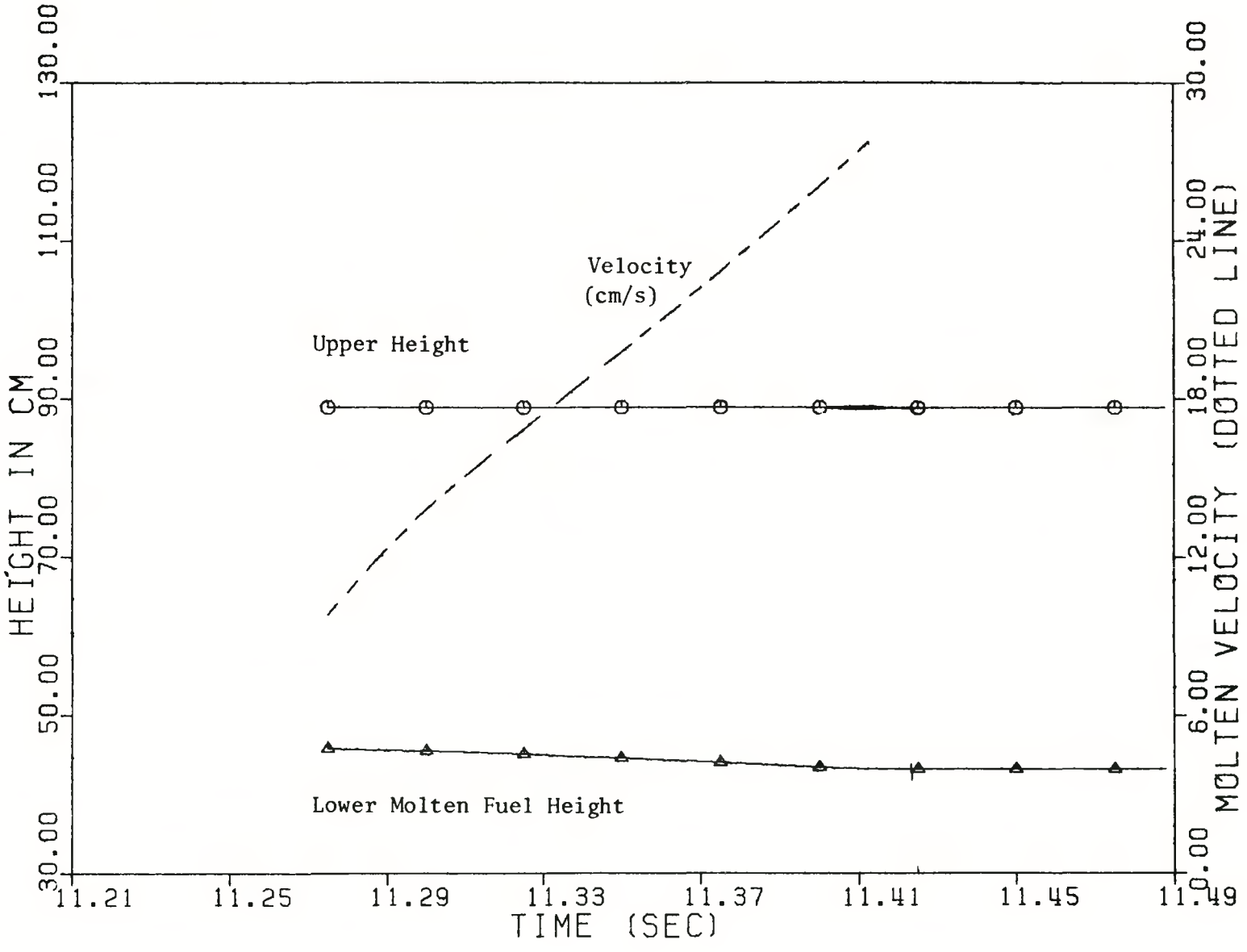

Figure 2.17 EOC1 Molten Fuel Height and Velocity
Channel 1 of Case E1.

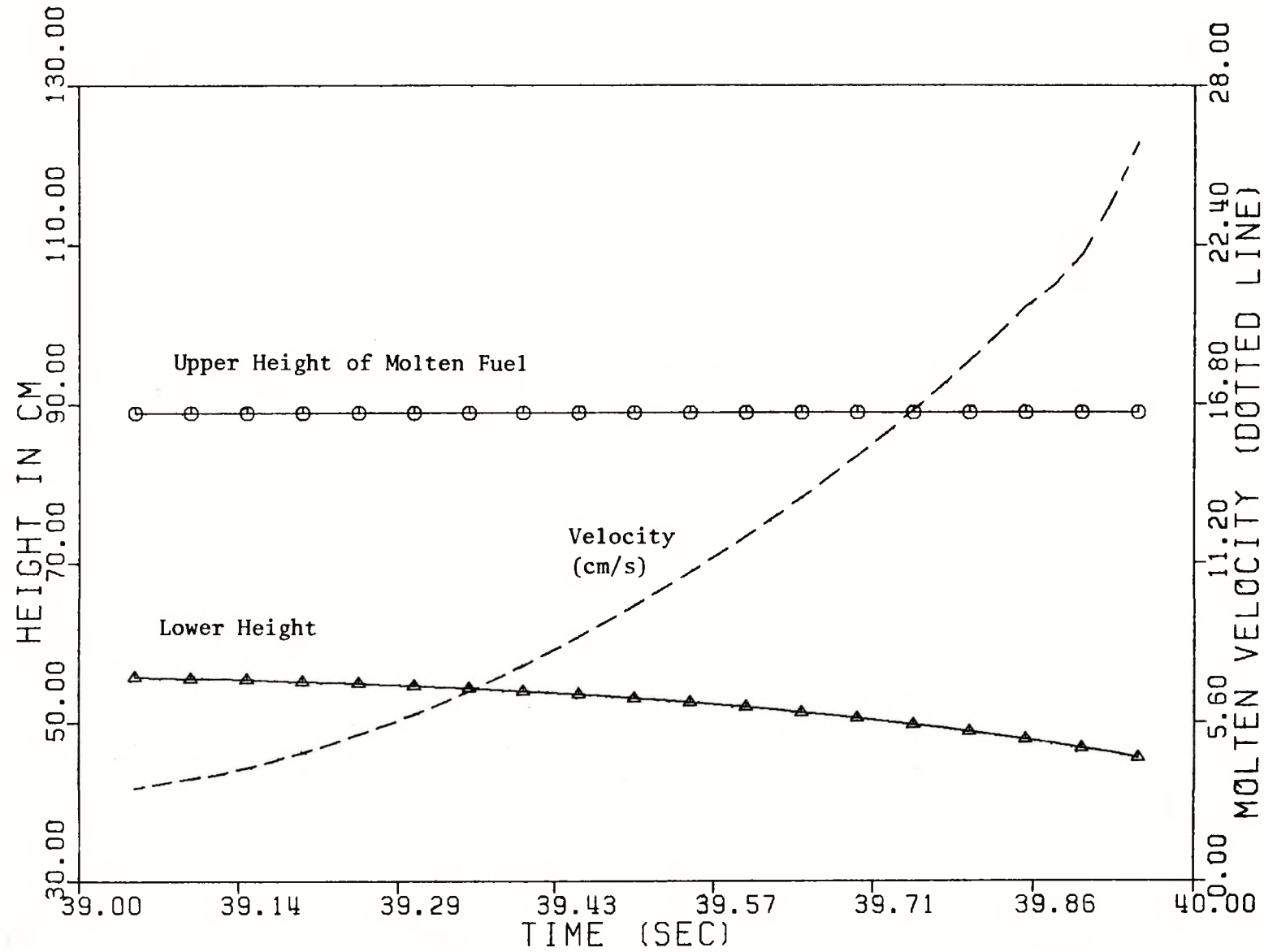

Figure 2.18 EOEC Molten Fuel Height and Velocity
For Channel 1 of Case E2.

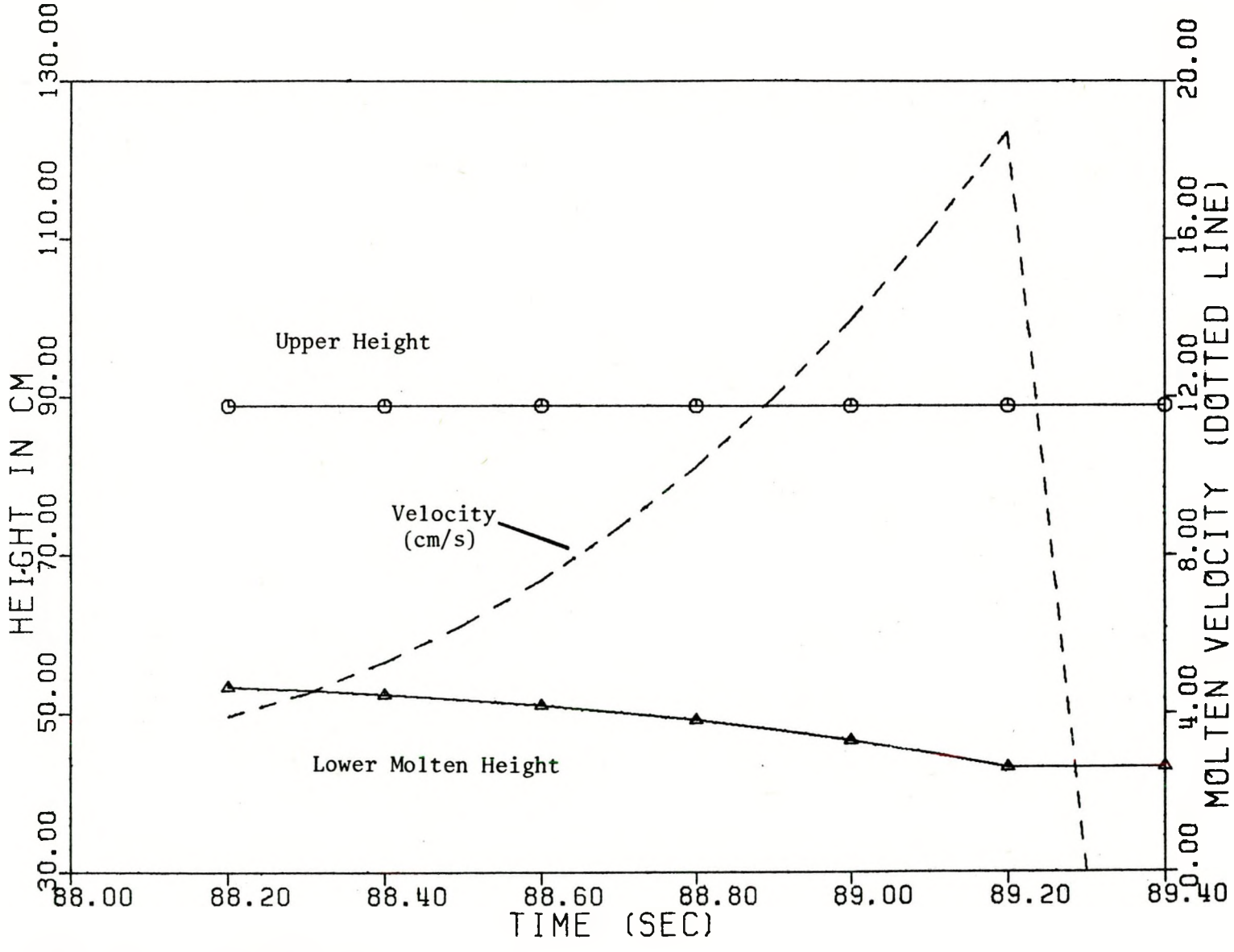

Figure 2.19 EOEC Molten Fuel Height and Velocity
For Channel 1 of Case E3.

References for Chapter 2.0

1. V. K. Dhir, J. Doshi, et.al., "LMFBR Fuel Analysis, Task A: Oxide Fuel Dynamics" NUREG/CR-0011, February 1978.

2. M. Frank, "Some Aspects of Fuel Rod Behavior During a Fast Reactor Overpower Excursion," Ph.D. Dissertation in Engineering, UCLA School of Engineering and Applied Science, December 1978.

3. A. E. Walter, A. Padella, Jr., and R. T. Shields, "Melt-III, A Two-Dimensional Neutronics-Heat Transfer Program for Fast Reactor Safety Analysis, "HEDL-TME 72-43, April 1972.

4. W. E. Kastenberg and M. V. Frank, "Preliminary Analysis of the Transient Overpower Accident for CRBRP," UCLA-ENG-7557, July 1975.

3. THERMAL-HYDRAULIC CONSIDERATIONS OF POROUS BLOCKAGES FORMED DUE TO FROZEN FUEL PARTICLES

3.1 Introduction

The transient overpower (TOP) accident is one of the two core disruptive accidents studied in conjunction with the safety of liquid metal fast breeder reactors. During the past several years computer codes such as HOPE [1], SAS [2], and PLUTO [3] have been developed, which model various physical phenomena that occur in the fuel pin and the coolant as a result of a positive reactivity insertion. Until recently, these computer models of transient overpower accidents have generally assumed that molten fuel injected into the coolant channels upon pin failure is swept out, thus adding strong negative reactivity to the core. This fuel sweep-out assumption is not supported by the TREAT H-4 and H-6 [4,5], where substantial in-channel fuel freezing and plugging of channels has been observed. However, it has been argued that in-channel plugging has occurred due to overdriving of the fuel pins in these tests (large amount of fuel injected into the coolant channel subsequent to first and second events). Out of pile single pin fuel injection tests have also been performed at ANL [6]. In the HUMP-1 test, substantial amounts of fuel freezing occurred but in test C2, the fuel injected in the early stages was completely swept out. The channel plugging in HUMP-1 test has been suggested to have occurred because the flow rate and pressure drop was considerably lower than prototypic. Increased flow rate and pressure drops associated with the C2 test are believed to have resulted in flow conditions favorable for fuel sweepout.

A mechanistic model for the description of in-channel fuel freezing and plugging was proposed in Reference [7]. In that case, a blockage of the type shown in Figure 3.1 was predicted to form when semi-molten fuel particles hit a wire wrap, break open and freeze on the wire wrap. Subsequently,

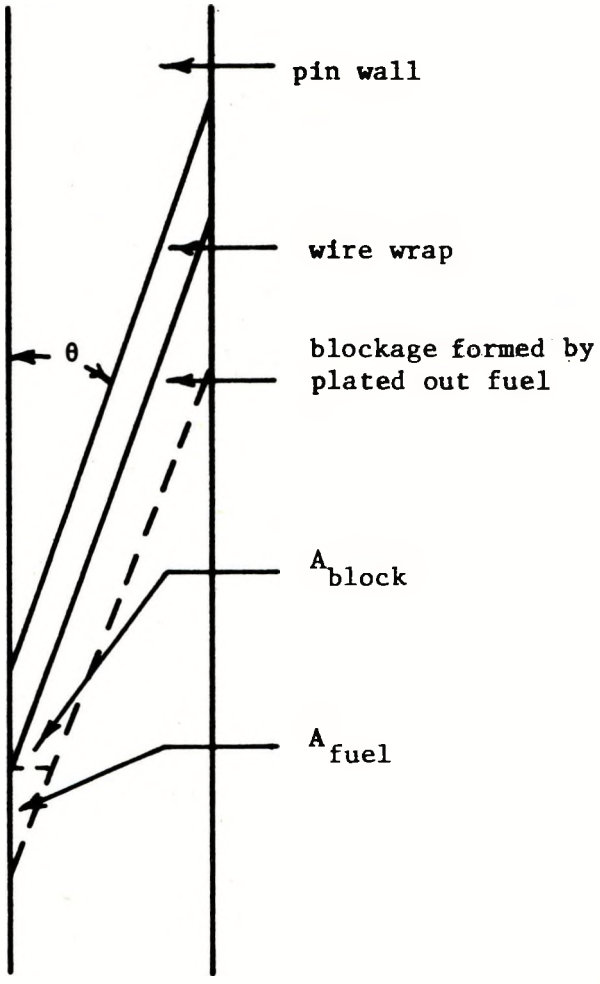

Figure 3.1 Blockages Formed by Freezing of Semi-Molten Fuel Particles.

a criterion [8] for the sticking of fuel to wire wrap or to an existing layer of solidified fuel was developed. Experimental observations were also made to determine the nature of the blockages that may be formed when solid fuel particles get stuck in the coolant channels. Figure 3.2 shows these blockages formed in the inside channels as well as in the channels next to the housing conecting the 7 pin fuel rod bundle.

Thermal loading of the type of blockages shown in Figure 3.1 was discussed in the last year's report [9]. In this work, thermal hydraulic characteristics of porous blockages of the type shown in Figure 3.2 are analyzed. In analyzing these blockages, it is assumed that the blockages are formed coherently so that they cover the entire subassembly. Consideration is given to blockages formed in the upper plane of the active core or in the upper blanket region. Generally plugging of the coolant channel would occur when the fuel particles are still very hot and the channel is voided. As coolant flow tries to re-establish in the channel, the coolant would have to pass through the blockage and thus strongly interact both thermally and hydraulically with the porous plug. This period of transient heat transfer in which the bulk of the stored energy generated during the accident is removed is of critical importance in assessing the potential for cooling of the porous blockage.

3.2 Hydraulic Characteristics of the Blockages

In the first instance, the thermal interaction of the porous plug with the fluid is neglected and the pressure drop across the porous plug, when either liquid or vapor flows through the plug, is considered. In obtaining the pressure drop across a plug of length L, Kozney-Carman equation with inertia terms included is written as

$$\frac{\Delta p}{L} = a\mu V + b\rho V^2 \qquad (1)$$

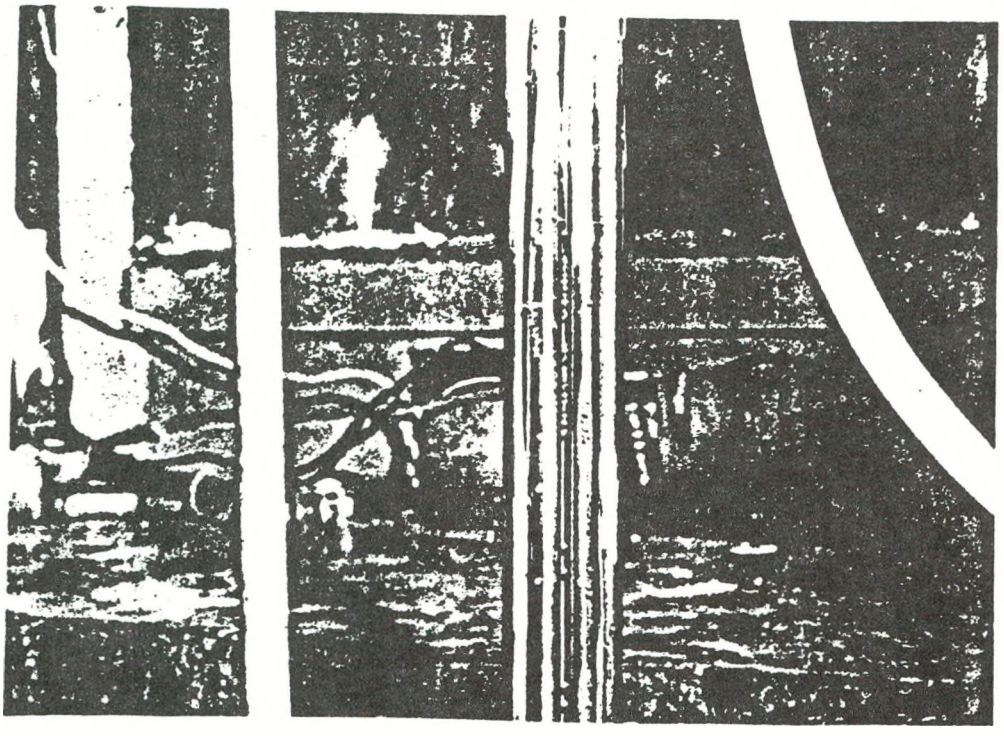

a. **Blockages Formed in Inside Channels**

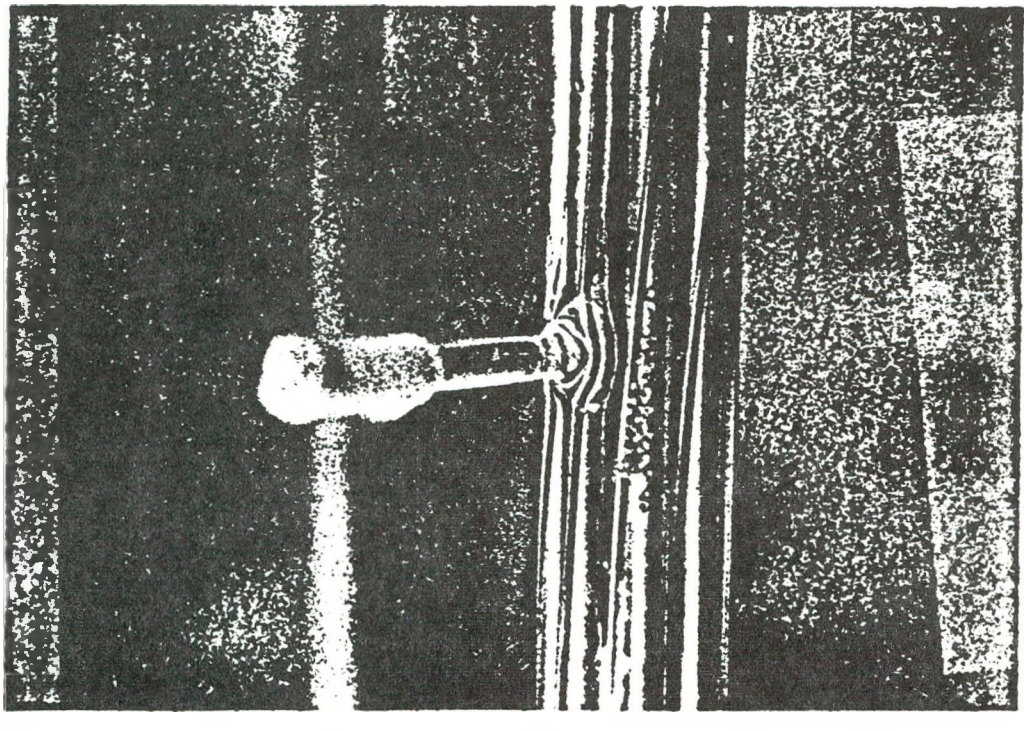

b. **Blockages Formed in Outside Channels**

Figure 3.2 Blockages Formed in Inside and Outside Channels When Solid Particles Get Stuck in the Channels

where the constants a and b are given by

$$a = \frac{150(1-\varepsilon)^2}{\varepsilon^3 d_p^2} \tag{2}$$

$$b = \frac{1.75(1-\varepsilon)}{\varepsilon^3 d_p} \tag{3}$$

In Equation (1) V, ρ, and μ are the velocity, density and viscosity of the fluid respectively. In Equations (2) and (3), ε, represents the porosity of the plug and d_p the mean diameter of the particles. Equation (1) has been obtained from the results of experiments with incompressible fluids [10]. However, it can, in conjunction with the gas law, be used for compressible fluids when acceleration effects are neglected.

Figure 3.3 shows the pressure drop across a 10 cm long porous plug having a porosity of 0.4 and a mean diameter of 100 or 1000 μM. The solid lines in Figure 3.3 correspond to the liquid velocity in the coolant channel below the plug and the dotted lines represent the pressure drop when an equivalent mass of vapor is assumed to flow through the plug. In plotting the pressure drop for vapor, the vapor density and viscosity are calculated at a pressure of 3 atmospheres. It is noted that for an available pressure drop of 6 atmospheres across a 10 cm long porous plug - with a porosity of 0.4, liquid sodium with an 'approach' velocity of 19 cm/sec could be maintained through the plug. This flow rate is of the same order as considered in SASBLOCK Code developed in support of Clinch River Breeder Reactor PSAR [11]. In performing the SASBLOCK calculations, the blockage was assumed thermally passive and only decay heat was removed by liquid sodium. For such a case it was concluded in the PSAR that core coolability under reduced flow conditions could be maintained. However, in reality the porous blockages may be very hot (thermally active) and liquid sodium

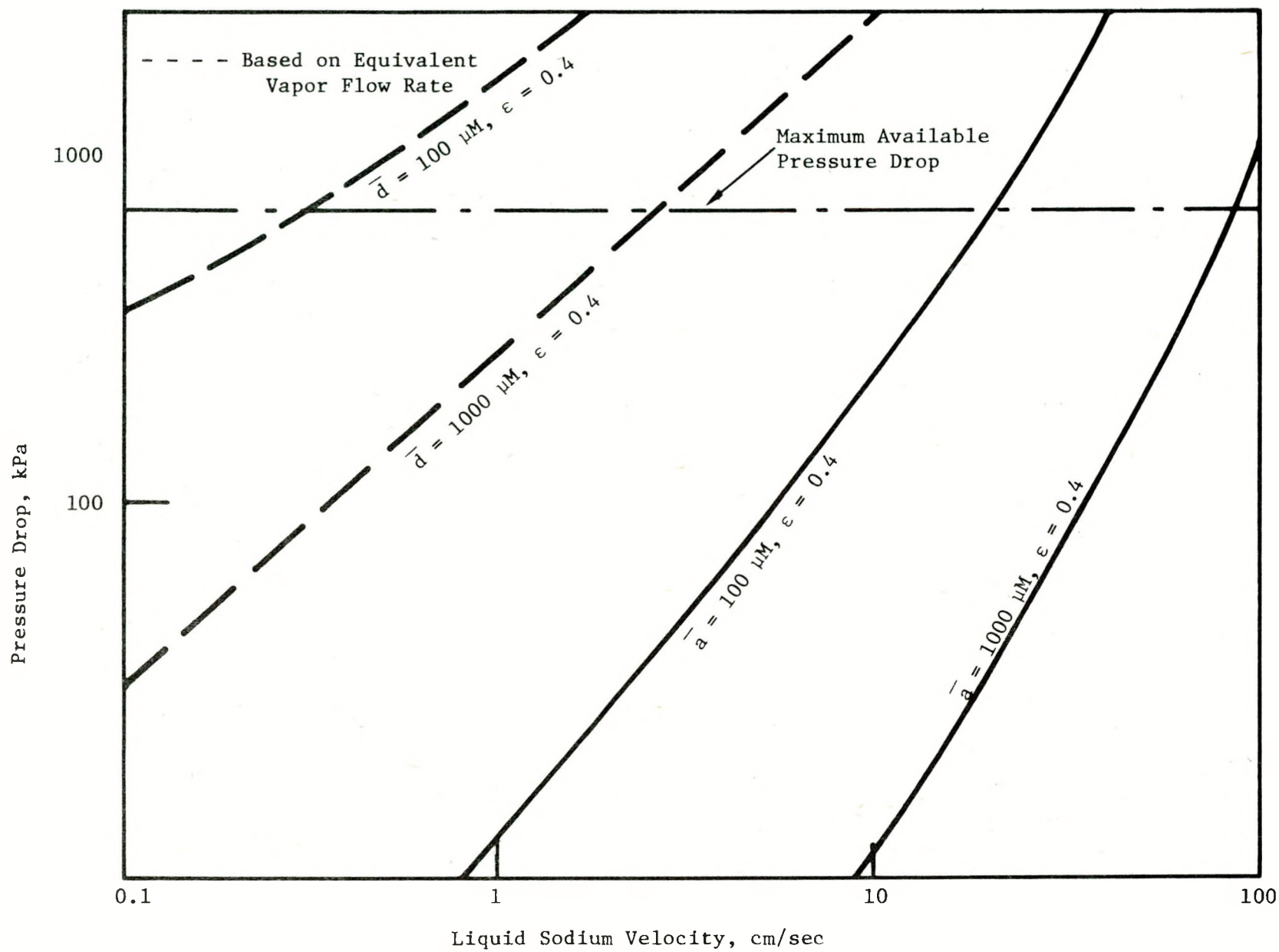

Figure 3.3 Frictional Pressure Drop Through a 10 cm long Porous Blockage

may change into vapor on entering the blockage. For such a case, a maximum liquid velocity of only 0.3 cm/sec could be maintained through the plug. Plugs of other diameters and porosities would behave in a similar way.

3.3 Thermal-Hydraulic Characteristics of Porous Blockage

Following the formation of a porous blockage in a voided channel, sodium flow will try to re-establish in the channel when the pressure in the voided region falls below the upstream pressure. As subcooled sodium enters the plug, it will be first heated to its saturation temperature. Thereafter, the energy transferred from the blockage will be utilized in phase change and subsequently the vapor will be superheated to the blockage temperature. In the porous medium, a very large surface area is available for transfer of heat from the praticles to sodium and in the liquid phase heat transfer region the blockage temperature will relax to the sodium temperature in times on the order of 3 millisec. The regions in which liquid sodium changes to complete vapor and is superheated to the blockage temperature has also been shown by Varela et.al. [12] to be very small (on the order of 10^{-3} cm and 10^{-1} cm, respectively). Thus, in general, a thermal equilibrium between solid particles and flowing sodium will be obtained very rapidly and little error would be made if liquid and vapor phases were assumed to be separated by a moving liquid vapor interface. Figure 3.4 shows the various flow regions that may be present when subcooled sodium enters a very hot porous plug.

In the absence of any flow oscillations in the blockage, the velocity of the liquid-vapor interface is determined by the rate at which liquid sodium enters the blockage and the rate at which vapor can leave the blockage under the available pressure drop. The vapor velocity, V_{VI}, above the interface, can be related to the liquid velocity $V_{\ell I}$ below the interface by making a mass balance as the liquid vapor interface moves

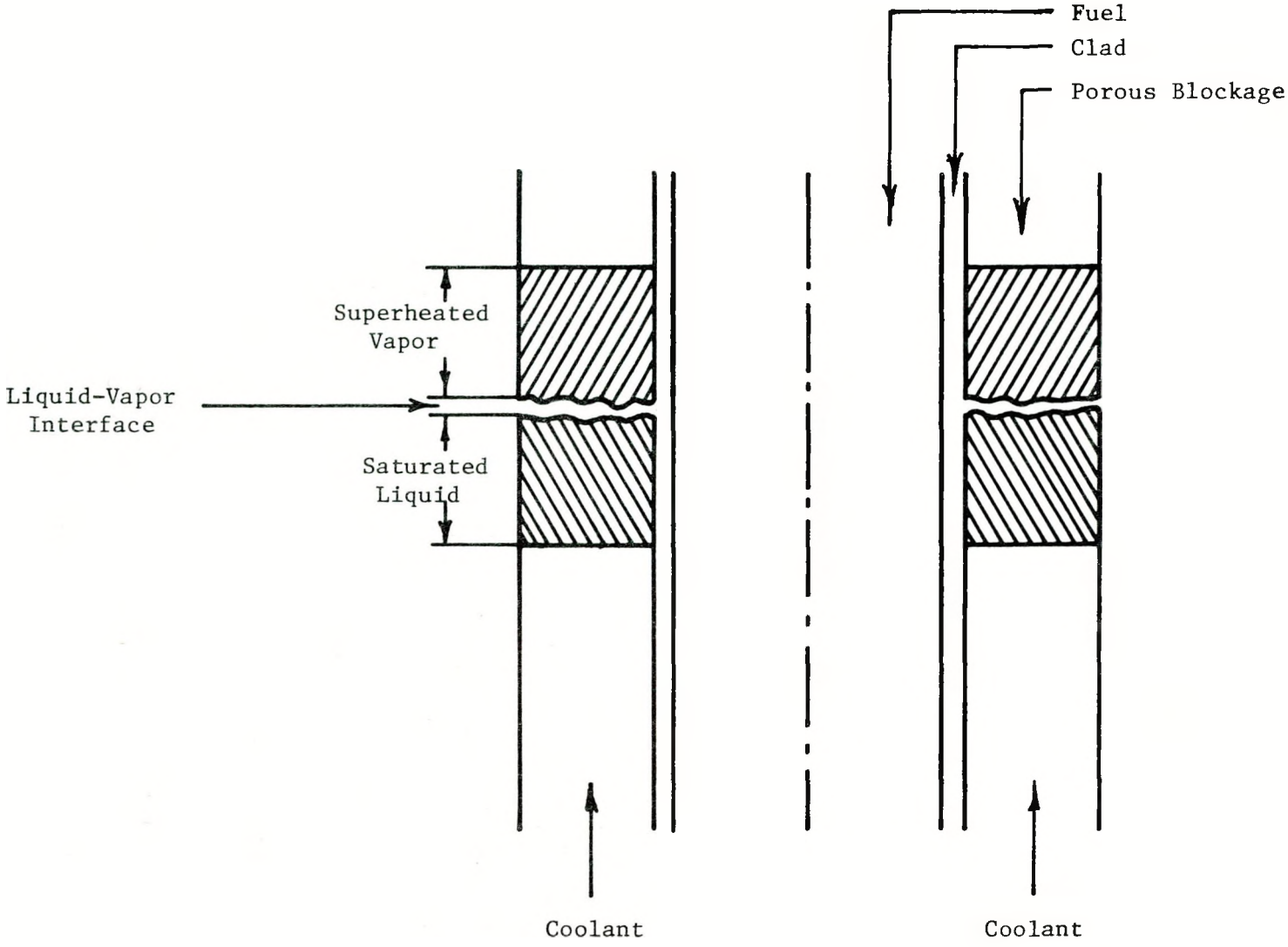

Figure 3.4 Model for Flow of Coolant Through The Porous Blockage

a distance dx:

mass into dx = mass out of dx + mass stored in dx

or,

$$\rho_{\ell I} V_{\ell I} dt = \rho_{VI} V_{VI} dt + \rho_{\ell I} V_I dt \qquad (4)$$

where V_I is the velocity of the interface.

The conservation of energy in element dx of the porous plug yields:

energy removed from plug of length dx = energy used to charge saturated sodium into vapor + energy used to superheat vapor to initial porous plug temperature [12]

or

$$(1-\varepsilon)(\rho c_p)_p (T_p - T^s_{\ell I}) V_I dt = (h_{fg} + c_{p_{VI}} (T_p - T^s_{\ell I})) \varepsilon \rho_{VI} V_{VI} dt \qquad (5)$$

In Equation (5) $(\rho c_p)_p$ represents product of density and specific heat of the porous plug, T_p the temperature of the blockage and $T^s_{\ell I}$ the saturation temperature of sodium.

By combining Equations (4) and (5), an expression relating the liquid velocity below the interface to the vapor velocity just above the interface is obtained as

$$V_{\ell I} = V_{VI} \left[\frac{\rho_{VI}}{\rho_{\ell I}} + \frac{\varepsilon}{1-\varepsilon} \frac{\rho_{VI}}{(\rho c_p)_p} \frac{(h_{fg} + c\rho_{VI} (T_p - T^s_{\ell I}))}{(T_p - T^s_{\ell I})} \right] \qquad (6)$$

The liquid velocity below the blockage, V_ℓ, is related to the liquid velocity below the interface, $V_{\ell I}$, in the porous plug by continuity:

$$V_\ell = \varepsilon V_{\ell I} \qquad (7)$$

The velocity of the coolant below the blockage and the velocity of the liquid-vapor interface as calculated in Reference [12] are shown in Table 3.1 for various particle diameters and porosities. The vapor exit

TABLE 3.1

Maximum Liquid Velocities in the Coolant Channel Below a 10 cm Long Porous Blockage*

Porosity	Particle Diameter (Micron)	Exit Vapor Velocity cm/sec	Interface Velocity cm/sec	Coolant Velocity in the Channel cm/sec
0.4	100	462	0.14	0.12
0.4	1000	3500	1.4	1.2
0.2	100	42	0.006	0.005
0.2	1000	840	0.15	0.12

* Initial porous blockage temperature is assumed to be 2500K

velocity has been fixed from an available pressure drop of 6 atmospheres over a 10 cm long plug. In obtaining the entries in Table 3.1, the blockage temperature has been taken to be 2500 K. It is noted from Table 3.1 that liquid velocities in the coolant channel are severely restricted by the resistance to vapor flow and are about 3 orders smaller than normal flow rate in CRBR subassembly. Increasing the particle diameter by a factor of 10 results in about a 10-fold increment in the liquid velocity below the blockage. Reducing the porosity of the porous blockage from 0.4 to 0.2 results in a 10-20 times reduction in the approach velocity of the coolant.

Severely restricted flow through the channel may result in bulk boiling of sodium in the coolant channel. To determine the undercooling experienced at the reduced flow rates, the heat transfer between the fuel pin and sodium flowing in the channel below the blockage is calculated. The one-dimensional heat conduction equation is used to calculate the transient temperature in the fuel, clad and the coolant. Axial conduction has been neglected and a Lagrangian approach is used in these approximate calculations.

The time dependent radial temperature profile in the fuel pin and the cladding (without gap) is obtained by solving transient conduction equation for a cylindrical geometry,

$$\rho c_p \frac{\partial T(r,t)}{\partial t} = \frac{1}{r} \frac{\partial}{\partial r} \left(k(T) r \frac{\partial T}{\partial r} \right) + Q \qquad (8)$$

The initial and boundary conditions are:

$$T(r,0) = f(r) \qquad \text{for all } r$$

$$\frac{\partial T(0,t)}{\partial r} = 0 \qquad \text{for all } t > 0$$

$$k_f \left.\frac{\partial T(r,t)}{\partial r}\right|_{r=r_c} = k_c \left.\frac{\partial T(r,t)}{\partial r}\right|_{r=r_c} \qquad \text{for all } t > 0 \qquad (9)$$

$$k_c \left.\frac{\partial T(r,t)}{\partial r}\right|_{r=r_o} = \bar{h}(T_o - T_\ell) \qquad \text{for all } t > 0$$

$$T_\ell(0) = T_\ell$$

For the coolant, conservation of energy gives:

$$A_c(\rho C_p)_\ell \frac{dT_\ell}{dt} = 2\pi r_o \bar{h}(T_o - T_\ell) \quad . \qquad (10)$$

Equations (8-10) are solved by using an implicit numerican scheme.

Following a transient overpower accident, the temperature at the center of the fuel pin above core midplane would be about the melting temperature of UO_2. It is difficult to apriori determine the temperature of the outer surface of cladding. It will depend in a complicated way on the flow and heat transfer conditions during the top accident. However, if local clad dryout does not occur the temperature of the cladding can be safely assumed to be about 20°C higher than that of liquid sodium. Thus, above equations have been solved for initial sodium temperatures of 660 k and 880 K while the initial fuel center temperatures are fixed to be either 3100 K or 2800 K [12]. The time required for the sodium to reach the saturation temperature when decay heat is assumed to be 50 watts/cm^3 (5% of average power of CRBR) is given in Table 3.2. Assuming that laminar flow of liquid sodium exists over the intact fuel pin, the heat transfer

Table 3.2 Time for Sodium to Reach Saturation State

Initial Fuel Center Temperature (°K)	Initial Clad Temperature (°K)	Initial Sodium Temperature (°K)	Time for Sodium to Reach Saturation State (sec)
3100	900	880	0.63
3100	680	660	1.22
2800	900	880	0.81
2800	680	660	1.79

oefficient has been taken to be 57 watts/cm^2 K. It is noted from Table 3.2 that for liquid sodium velocities of about 1 cm/sec, the time needed for boiling to occur in the channel is of the order of 1 second only.

During this time, the liquid-vapor interface in the porous blockage of length 10 cm, particle diameter 1000 μM and a porosity of 0.4 would move only about 1 cm. Thus, sodium will boil and void the channel below the blockage before any significant portion of the blockage can be cooled. In obtaining the reduced steady state sodium flow rates in the coolant channel, it is assumed that sodium can penetrate through the porous plug. Evidently there could be situations when vapor generation rate may exceed the rate that is possible with the available pressure drop. In such a case, a buildup of pressure in the plug will reduce the coolant flow and possibly expel sodium out of the coolant channel. This in turn may reduce or completely eliminate cooling of the plug by flow of sodium through the plug.

3.4 Thermal Considerations

Because of complicated boundary conditions at the porous plug and uncertainty in the composition of the blockage (steel and UO_2) it is difficult to precisely determine the thermal behavior after porous plug. However, conservative estimates of the time in which the blockage may remelt under given decay heat generation rates can be made. Using a lumped capacity method, the rate of temperature rise of the porous plug can be written as:

$$(\rho C_p)_p \frac{dT_p}{dt} = Q \qquad (11)$$

Solution of equation (11) for decay heat source strength of 50 w/cm^3 (5% of average power in CRBRP) yields that the porous plug with initial temperature of 2500 K will start to melt after about 1/2 second. In solving equation (11) it has been assumed that no heat is lost from the plug and thus, estimated melting time is conservative.

Thermal history of porous blockage using one dimensional radial heat flow model has been obtained by Varela et.al. [12]. In that model, heat losses to flowing sodium vapor are neglected and temperature in the center of the fuel plug is assumed to be 3100 K while the outer surface temperature of plug is assumed to be 1000 K. For a porous plug located in the active core region, it is noted that the plug will start to melt after about 2 1/2 minutes, when decay heat is 5% of full power in CRBRP. However, if the plug is located in the upper axial blanket region, it may take 5 to 10 minutes for melting to initiate in the central region of the plug.

3.5 Conclusions

1. Core coolability without boiling may be obtained if the porous blockage formed in the core after TOP accident is thermally passive (cold).
2. Thermally active (hot) blockages formed in the core may reduce flow of coolant in the channel by 3 orders of magnitude as compared to the normal flow in CRBRP. This is mainly due to excessive resistance encountered by the vapor as a result of thermal interaction of liquid sodium with hot fuel particles in the blockage.
3. Severely restricted flow conditions in the coolant channel may lead to bulk boiling of sodium in the channels below the blockage after about 1 second. During this time, liquid sodium would have penetrated about 1 cm into the porous blockage having 1000 μM diameter particles and a porosity of 0.4.
4. As a result of bulk boiling of sodium beneath the blockage, coolability of the porous blockage may be severely limited. Such a blockage, if formed in the active core region, may start to re-melt in times of the order of one minute. However, if the blockage is formed in the upper axial blanket, the melting may be delayed to about 5-10 minutes.

REFERENCES FOR CHAPTER 3.0

1. Rumble, E. T., III, "A Hypothetical Overpower Excursion Model for Liquid Metal-Cooled Fast Breeder Reactors," Ph.D. in Engineering, University of California, Los Angeles, June 1974.

2. Smith, L.L., et.al., "SAS/FCI, a Fuel-Coolant Interaction Model for LMFBR Whole-Core Accident Analysis," Proc. ANS Topical Mtg. on Mathematical Models and Computation Techniques for Analysis of Nuclear Systems, Ann Arbor, Michigan, April 1972, USAEC CONF-730414-P1, pp. 137-158.

3. Wider, H. U., J. F. Jackson, L. L. Smith, and D. T. Eggen, "An Improved Analysis of Fuel Motion During an Overpower Excursion," Proc. ANS Conf. on Fast Reactor Safety, Beverly Hills, California, April 1974, USAEC CONF-740401, pp. 1541-1555.

4. Wright, A. E., "Transient Overpower Test H-4," Argonne National Laboratory, ANL/RAS 74-30, November 1974.

5. Page, R. J., A. B. Rothman, K. J. Schmidt, C. L. Fink, R. W. Morning, R. K. Lo, P. H. Froehle and E. W. Johnson, "TREAT TOP Test H-6-Preliminary Results," ANS Transactions, Vol. 28, 1978, pp. 481-82.

6. Spencer, B. W., L. Bova, G. T. Goldfuss, D. Ragidon, R. E. Henry and D. R. Armstrong, "CAMEL Single Pin Fuel Sweepout Test C_2, "ANS Transactions, Vol. 27, 1977, pp. 503-04.

7. Wong, K. W., V.K. Dhir, and W. E. Kastenberg, "A Study of Fuel Freezing and Channel Plugging During Hypothetical Overpower Transients," Proc. of Intl. Mtg. on Fast Reactor Safety and Related Physics, Chicago, October 1976, U.S. ERDA 7610001.

8. Wong, K. W., V. K. Dhir, and W. E. Kastenberg, "A Mechanistic Study of Fuel Freezing, Channel Plugging, and Continued Coolability During Fast Reactor Overpower Excursions," Nuclear Technology, Vol. 39, July 1978, pp. 121-137.

9. Dhir, V. K. et.al., "LMFBR Fuel Analysis Task A: Oxide Fuel Dynamics" NUREG/CR-0011, 1977.

10. Carman, P. C., "Fluid Flow Through Granular Beds," Transactions of Institute of Chemical Engineers (London) Vol. 15, 1937, pp. 150-166.

11. Preliminary Safety Analysis Report, Clinch River Breeder Reactor, Project Management Corporation, 1975.

12. Varela, D., W. E. Kastenberg and V. K. Dhir, "Implications of In-Channel Plugging During Fast Reactor Overpower Excursions," Paper submitted to Nuclear Technology.

4. ALTERNATE FUEL CYCLES

4.1 Introduction

During the past year, there has been renewed interest in potential alternatives to the mixed oxide $(U,Pu)O_2$ fuel cycle for the Liquid Metal Fast Breeder Reactor (LMFBR) and the Light Water Reactor (LWR), [1-3]. These alternatives include thorium based fuels [4], mixed carbides (U,Pu)C and nitrides (U,Pu)N [5], and the Canadian CANDU system [6].

In this chapter, background information which can later be used for initial studies of LMFBR safety with thorium based fuels is presented. Such fuels include:

$(Th,U)O_2$	$(Th,U,Pu)O_2$
(Th,U)C	(Th, U,Pu)C
(Th,U) metal	(Th,U,Pu) metal.

As stated by Sehgal et.al. [1], interest in the thorium-based fuel cycle in fast breeder reactors (FBRs), (as shown in the first column) had been quite strong historically. However, the interest subsided because of its lower breeding potential compared to that of mixed oxide in a fast spectrum. Symbiotic (or mixed-progeny) fuel cycles (as shown in the second column) may also be attractive because they use both primary fuel resources (natural uranium and thorium). Another candidate is the so-called "denatured" thorium fuel cycle.

The denatured thorium fuel cycle has been suggested by Feiveson and Taylor [7] as a method of mitigating the potential for weapons proliferation. As is well known, ^{233}U is a perfectly good weapons material with a critical mass somewhat less than plutonium, and with no pre-ignition problem [4.h]. Feiveson and Taylor [7] suggest a mixture of ^{233}U (12.5%) with ^{238}U (87.5%). This could be accomplished after breeding the ^{233}U

or preferably, from the safeguards viewpoint, beforehand, by intimately mixing the ^{232}Th and ^{238}U[4.h]. This prevents the isotopic separation of the fissile material by chemical means.

This chapter covers two points: safety related physics, and accident analysis and research needs.

4.2 Safety Related Physics

The state of the art concerning safety related physics is summarized in References 1, 3, 4 and 8 and will be briefly summarized here.

Doppler Coefficient

Sehgal et.al. [1], presents a series of calculations for spherical and cylindrical shaped cores fueled with (Th,U) or (Th,Pu,U). The spherical cores were based on a 2500 MW(th)/1000 MW(e) reactor with Vanadium-20 Titanium clad for the metal fuel and 316SS for the oxide fuel. Metal fueled cores with sodium coolant had Doppler coefficients (T dk/dT) of -0.009, while with helium the Doppler coefficient was -0.007. to 0.010, depending upon the blanket (Thorium-metal or Uranium-metal). The oxide cores had Doppler coefficients between -0.014 and -0.016 for sodium coolant and -0.010 for helium coolant.

The cylindrical cores were sodium cooled, metal or oxide fueled cores, with UO_2 and ThO_2 axial blankets. These Doppler constants varied between -0.0078 and -0.0093.

Sodium Void Coefficient

A number of different calculations of sodium void coefficients for Thorium based fuels have been presented recently [1,4.i,4.j]. For spherical cores with a thorium metal based fuel, and thorium metal blankets, whole core sodium voiding produced a change in multiplication of -4.60% with (U,Th) and -2.29% with (U,Pu,Th). With (U,Pu,Th) and a uranium

metal blanket, the change in miltiplication was -0.71%. With oxide fuel, the voiding of sodium produced a positive effect, varying between +0.01 and +0.39% in Δk. A conventional mixed oxide core had a sodium void of +3.73% in Δk.

The cylindrical cores with plutonium (metal or oxide) had sodium void effects between +0.39% and +0.92% (in Δk) for the inner core and -0.73% to -0.52% (in Δk) whole core. For (U,Th), the inner core had a -0.49% Δk for the inner core and -2.25% Δk for whole core sodium voiding. A conventional mixed oxide core had +2.71% and +3.25% respectively for inner and whole core sodium voiding.

D. R. Marr et.al. [4.i] considered the performance of various thorium fueled LMFBR designs. The first comparison involved two small breeder designs, one using thorium oxide, the other thorium metal, both with ^{233}U enrichment. The second compared a 1200 MW(e), (PuU) O_2 design to a 1200 MW(e) (Th,U) metal design. The third compared the performance of thorium metal and thorium oxide radial blankets for three large breeders using uranium oxide or thorium oxide cores.

In the first comparison (for the small cores) the sodium void was worth -3\$ in either case (or $\sim$ -0.006 in Δk). In the second comparison, the (Th,U) metal core exhibited a void worth of -2.1\$ while the $(Pu,U)O_2$ exhibited a void worth of +4.28\$. Sodium void calculations were not reported for the third comparison.

Haffner, et.al. [4.j] reports on reactor physics calculations for a typical 1200 MW(e), FBR design with (a)U^{233} substutited for ^{239}Pu as a fissile fuel and/or (b)^{232}Th substituted for ^{238}U as the fertile fuel. Eight configurations were studied, all with oxide fuel. The four configurations with ^{239}Pu as the fissile fuel resulted in a Δk for sodium voiding

in the core ranging between -0.0023 and -0134; the latter with (U,Th) in the core and thorium oxide in both the radial and axial blanket.

Other Considerations

In a thorium based fuel there may be a considerable buildup of ^{232}U, among whose daughters there are some strong γ-ray emitters. The principle paths are the (n,2n) and (n,γ) reactions in ^{232}Th and the (n,2n) reaction in ^{233}U. The relative biological hazard for ^{232}U compared to ^{239}Pu will be greater. The half life of ^{239}Pu is $3x10^3$ times greater and its total (all daughters) alpha activity is 6 times lower. Hence, gram for gram, the ^{232}U would exhibit a greater biological hazard by a factor of $1.8x10^3$ than ^{239}Pu. Some preliminary calculations indicate that the amount of ^{232}U produced in thorium based LMFBRs may be significant [9].

It should also be pointed out that the delayed neutron fraction for ^{233}U is smaller than for ^{239} Pu. This affects the reactor period and rate of power increase below prompt critical.

4.3 Accident Analysis and Research Needs

The limited amount of analysis and data is best reflected by the following general comments which appeared in a recent Argonne National Laboratory monthly report [10]:

$(Th,U)O_2$: No data base. Behavior is expected to be similar to that of $(U,Pu)O_2$. Effects of different physical properties and chemistry need to be assessed.

(Th,U)C: No data base. Very limited data for UC and/or (U,Pu)C systems.

(Th,U) metal: Very limited data base. Some guidance from extrapolations based on EBR-II driver fuel data.

The behavior of EBR-II driver fuel and its potential extrapolation to Th-U metallic fuel has been discussed recently by Seidel, et.al.[11].

In addition, a special session on "The Materials Technology of Thorium Fuels" was held at the November, 1977 meeting of the American Nuclear Society [12]. The session further reflects the lack of a comparable data base to $(Pu,U)O_2$. However, some preliminary information regarding fission product behavior (swelling and gas release) was reported [12d,e].

Transient Overpower Accident

The major safety issues for mixed oxide fuel are applicable to any alternate system:

a) Time, place and mode of pin failure;

b) Post-Failure fuel/coolant dynamics (including molten fuel coolant interactions), fuel freezing and channel plugging;

c) Disassembly and work energy;

d) Ultimate core coolability and/or post accident heat removal.

The time, place and mode of fuel pin failure will in all probability be different for different fuel choices. First, the melting and vaporization temperatures will be different as shown below [10]:

	Temperature °C	
Fuel	Melting	Vaporization
$(UPu)O_2$	2,700	3,400
$(Th,U)O_2$	∿ 3,400	4,000
(Th,U)C	∿ 2,400	4,400
(Th,U)metal	∿ 1,400	4,600

Second, the fission gas behavior in each fuel will probably be different. Using the $(U,Pu)O_2$ as a reference, the (Th,U)C may be highly gas retentive, as is (U,Pu)C. Fission gas release as a function of fuel swelling is characteristically the same for all metal fuels as a consequence of the development of interconnected porosity at ∿ 33% fuel swelling [11].

Fission gas release data for $(Th,U)O_2$ fuels irradiated as part of the LWBR Irradiations Test Program were recently reported by Goldberg et.al [12e.]. Because of the higher thermal conductivity of the thorium based fuels, the fuel samples may be run at lower peak temperatures. In this program fission gas release data were obtained from 51 ThO_2 and ThO_2 - UO_2 LWBR fuel rods that experienced peak linear power ratings from 2.2 to 22.5 kW/ft and peak burnups from 900 to 56,500 MWd/MT (U+Th). Measured gas release ranged from 0.1 to 5.2%, much less than typical UO_2 fuels.

Post-failure fuel/coolant dynamics are highly dependent on the thermo-physical properties as well as the amount of fission gas present. Higher conductivity fuels may have a higher propensity for freezing and an abundance of fission gas may inhibit fuel fragmentation. Higher conductivity fuels may be more conducive to molten fuel/coolant interactions, if their melting point is sufficiently high.

The potential for disassembly, should fuel sweepout not be effective, will depend on positive insertions of reactivity. With negative void coefficients and large negative Doppler coefficients, one would expect them to be mild.

On the other hand, higher thermal conductivities as well as other thermophysical and chemical properties may cause PAHR requirements to change significantly.

Loss of Flow Accidents

Loss of flow accidents with alternate fuels may be considerably different from those described with the conventional mixed oxide fuel. Of particular importance is the role of a negative sodium void coefficient. For the $(Th,U)O_2$ fuel, with a negative void coefficient, an unprotected loss of flow accident may resemble a loss of heat sink accident, starting

at low power. Following voiding, eventual dryout would occur due to decay heat generation. Uncovering the core, which would be subcritical, could lead to a slow progression to melting and eventual core slumping would lead to re-criticality considerations.

For both the carbide and metal fuels, the melting point occurs well below the boiling point of steel. In addition, the melting point of $(Th,U)_{metal}$ is roughly 1,400 °C, very close to the melting point of 316 20% CW stainless steel. Hence, fuel failure, disruption and/or collapse could yield different reactivity effects and/or their importance heightened in the absence of a positive sodium void coefficient.

Gassy fuels (such as carbides) may exhibit a potential for early fuel dispersal so that accident energetics could change. PAHR requirements may also be different.

4.4 Conclusions

The research needs, vis-a-vis safety, for alternative fuels are similar to those prepared for the "advanced fuels" (U,Pu)C and (U,Pu)N discussed in Reference [13]. The situation is somewhat acute because of the absence of a sound data base. Almost all aspects of LMFBR safety concerned with core disruption and fission product release rely on fuel pin behavior. The U.S. program has focused on mixed oxide $(U,Pu)O_2$ with some tests on mixed carbide (U,Pu)C and nitride (U,Pu)N; the latter steady state irradiations. Virtually no data exists for $(Th,U)O_2$ and (U,Th)C. Metallic fuels are better known because of early experience in EBR-II and FERMI, but must be extrapolated (a great deal) for present day considerations.

Because of the potential for a negative sodium void coefficient, the character of HCDA's will drastically change. Consequence analysis will also be quite different because fission gas (product) release and retention will also be significantly different and the nature of the

transuranics will be different. Lastly, post accident heat removal and core retention will change because of the differences in thermo-physical properties.

REFERENCES FOR CHAPTER 4.

1. Sehgal, Bal Raj, et.al. "Thorium Based Fuels in Fast Breeder Reactors," Nuclear Technology, 35 p. 636.

2. Chang, Y. I., et.al. "Alternate Fuel Cycle Options," Argonne National Laboratory, ANL-77-70, September 1977.

3. Williams, C.D. "A Review of Nuclear Fuel Cycle Alternatives Including Certain Features Pertaining to Weapons Proliferation," Sandia Laboratories, SAND-77-1727, January 1978.

4. Transactions of the American Nuclear Society. Session on "Thorium Fuel Cycle Potential in a Breeder Economy," Vol 27, pp 957-970, November 1977.

   a. R. A. Karam, "The ^{233}U- ^{232}Th Fuel Cycle as an Alternative to LMFBR's."

   b. P. Kasten and D. E. Bartine, "The Role of Thorium Fuel Cycles."

   c. Y.E. Chang et.al. "Performance Characteristics of Thorium Cycle in CANDU Reactors and LMFBR's."

   d. M. J. Driscoll, "The Use of Thorium in LMFBR Blankets"

   e. B. R. Sehgal et.al., "Performance of Various Fuel Cycles Based on Thorium in LMFBR's."

   f. C. J. Hamilton et.al., "The thorium cycle in Fast Breeders and Thermal Convertors."

   g. C. A. Sege et.al. "The Denatured Thorium Cycle - An Overview."

   h. C. M. Newstead, "Denatured Thorium Fuel Cycle Safeguards."

   i. D. R. Marr, et. al., "Performance of Thorium-Fueled Fast Breeders."

   j. D. R. Haffner and R. W. Hardie, "Reactor Physics Parameters of Alternative-Fueled FBR Core Designs."

5. Galluzzo, N.G., et.al. "Advanced Fuel Core Designs for CRBRP." Transactions of the American Nuclear Society, Vol 27, pp 754-756, November 1977.

6. Van Erp, Jan B., "Preliminary Evaluation of Licensing Issues Associated with U.S. Sited CANDU-PHW Nuclear Power Plants", Argonne National Laboratory, ANL-77-97, December 1977.

7. Feiveson, H.A. and Taylor, T.B. "Security Implications of Alternative Fission Futures." Bull. Atomic Scientists, Dec. (1976).

8. Ludewig, H., Memorandum to R. J. Cerbone, Brookhaven National Laboratory, December 15, 1977.

9. Mann, F.M., and Schenter, R. E., "Production of Uranium 232 in a 1200 MW(e) LMFBR," Nuclear Science & Engineering, Vol 65, #3, March 1978, pp 544-547.

10. Reactor Development Program, ANL-RDP-67, January 1978, pp 6.1-6.6.

11. B. R. Seidel, R. E. Einziger and C. M. Walter, "Th-U Metallic Fuel: LMFBR Potential Based on ERB-II Driver Fuel Performance", ANS Transactions, Vol 27, pp 282-283, November 1977.

12. Transactions of the American Nuclear Society. Session on "Materials Technology of Thorium Fuels," Vol 27, pp. 303-313, November 1977.

a. R. W. Jones, et.al. "Thoria Fuel Technology for CANDU-PHW Reactors

b. A. D. Lane et.al., "Fuel Technology for Denatured Thorium Cycles in CANDU Reactors.

c. A. W. Weinrich, et.al., "Fabrications of High Density, High Integrity Thoria Base Fuel Pellets."

d. A. S. Bain, et.al., "Performance of ThO_2 - UO_2 Fuel Irradiated in the NRU Reactor at CRNL.

e. I. Goldberg et.al., "Fission Gas Release from Th O_2 and ThO_2-UO_2 Fuels.

f. O. M. Stansfield et.al., "Performance of ThO_2 in HRGR Fuel Particles".

g. H. B. Meireran and E. L. Westermann, "An Evaluation of the Performance of ThO_2-UO_2 in a Large PWR-Type Fuel Rod Using the LIFE-THERMAL Computer Code."

h. W. B. Loewenstein and B. R. Sehgal, "Realities of Utilizing Thorium-Based Fuels in LWR's and LMFBR's."

13. W. E. Kastenberg, "Safety Research Needs for Carbide and Nitride Fueled LMFBR's," UCLA-ENG-7545, June 1975.

NRC FORM 335 (7-77)

U.S. NUCLEAR REGULATORY COMMISSION

BIBLIOGRAPHIC DATA SHEET

1. REPORT NUMBER *(Assigned by DDC)*: NUREG/CR-0721

4. TITLE AND SUBTITLE *(Add Volume No., if appropriate)*:
LMFBR FUEL ANALYSIS
TASK A: OXIDE FUEL DYNAMICS

2. *(Leave blank)*

3. RECIPIENT'S ACCESSION NO.

7. AUTHOR(S):
V. K. Dhir, M. Frank, W. E. Kastenberg, T. E. McKone

5. DATE REPORT COMPLETED
MONTH: March | YEAR: 1979

9. PERFORMING ORGANIZATION NAME AND MAILING ADDRESS *(Include Zip Code)*:
University of California at Los Angeles
Department of Chemical, Nuclear and Thermal Engineering
Los Angeles, California 90024

DATE REPORT ISSUED
MONTH | YEAR

6. *(Leave blank)*

8. *(Leave blank)*

12. SPONSORING ORGANIZATION NAME AND MAILING ADDRESS *(Include Zip Code)*:
U. S. Nuclear Regulatory Commission
Office of Nuclear Reactor Regulation
Division of Project Management
Washington, D. C. 20555

10. PROJECT/TASK/WORK UNIT NO.

11. CONTRACT NO.
NRC-03-77-001

13. TYPE OF REPORT: Technical

PERIOD COVERED *(Inclusive dates)*: October 1, 1977 - September 30, 1978

15. SUPPLEMENTARY NOTES

14. *(Leave blank)*

16. ABSTRACT *(200 words or less)*

Three aspects of liquid metal fast breeder reactor safety are discussed, namely (1) the potential reactivity effects of whole core fuel motion prior to pin failure in low ramp rate transient overpower accidents; (2) the effects of flow blockages following pin failure on the coolability of a core following an unprotected overpower transient; and (3) safety-related implications of using thorium based fuels. Results show that (1) prefailure fuel motion has a larger reactivity effect at high burnups because of the larger central cavity; (2) following a transient overpower accident restricted flow conditions may lead to bulk boiling of sodium in channels below the blockage on the order of one second, thereby severely limiting coolability of the porous blockage; and (3) lack of data is a major problem in determining safety implications of using thorium based fuels. Reactor physics calculations indicate a strong negative Doppler coefficient for thorium based fuels and generally negative sodium void coefficients. Loss of flow accidents with negative void coefficients may take on a very different behavior than conventional systems with mixed oxide fuel.

17. KEY WORDS AND DOCUMENT ANALYSIS

17a. DESCRIPTORS

17b. IDENTIFIERS/OPEN-ENDED TERMS

18. AVAILABILITY STATEMENT
NO RESTRICTIONS ON AVAILABILITY

19. SECURITY CLASS *(This report)*: Unclassified

21. NO. OF PAGES

20. SECURITY CLASS *(This page)*: Unclassified

22. PRICE: $

NRC FORM 335 (7-77)